Pressure Tube-Calandria Tube Thermal Contact Conductance

PRESSURE TUBE-CALANDRIA TUBE THERMAL CONTACT CONDUCTANCE

BY

ADAM CZIRAKY, B.Sc.

A THESIS

SUBMITTED TO THE DEPARTMENT OF ENGINEERING PHYSICS

AND THE SCHOOL OF GRADUATE STUDIES

OF MCMASTER UNIVERSITY

IN PARTIAL FULFILMENT OF THE REQUIREMENTS

FOR THE DEGREE OF

MASTER OF APPLIED SCIENCE

Master of Applied Science (2009)
(Engineering Physics)

McMaster University
Hamilton, Ontario, Canada

TITLE: Pressure Tube-Calandria Tube Thermal Contact Conductance

AUTHOR: Adam Cziraky
B.Sc., (Engineering Physics)
Queen's University, Kingston, Canada

SUPERVISOR: Dr. John Luxat

NUMBER OF PAGES: xiv, 106

To my Parents

Abstract

CANDU reactors are of the heavy water moderated, pressure tube type. The core consists of several hundred horizontal fuel channels surrounded by a heavy water moderator. Fuel channels consist of a Zircaloy-2.5%Nb pressure tube enclosed within a Zircaloy-2 calandria tube. There is an annulus gas gap between the pressure tube and the calandria tube. Under extreme accident conditions such as a critical break Loss Of Coolant Accident (LOCA), the pressure tube may deform. If the fuel channel remains pressurized, the hot pressure tube can balloon into contact with the calandria tube.

Thermal contact conductance between the pressure tube and calandria tube must be understood as it is a key factor in studying fuel channel integrity. Once PT-CT contact occurs, heat is transferred from the hot pressure tube to the relatively cool calandria tube. The heat flux to the calandria tube is a function of the temperatures of the two tubes as well as the thermal contact conductance between them. For high heat flux levels the calandria tube temperature can increase enough for film boiling to occur on the outer surface. Film boiling will severely limit heat transfer to the moderator and cause overheating of the calandria tube which could lead to fuel channel failure. It is therefore important to understand the mechanisms involved in thermal contact conductance and to study the transient behaviour of contact conductance during a

PT-CT contact event.

This paper presents a new approach to calculating the contact conductance transient during the initial contact and post-contact phases of a postulated critical break loss of coolant accident. The contact pressure at the interface between the tubes is a critical parameter in determining the thermal contact conductance. An iterative method is used to solve for creep strain in the pressure tube and calandria tube which determines the interfacial pressure. A modern correlation for contact conductance is then applied. The results show high contact conductance at first contact in the initial contact phase. This is followed by a rapid decrease in conductance across the interface. These results are due to the interfacial pressure being high at initial contact. In the post contact phase, as the pressure tube transfers heat to the calandria tube and cools down, thermal expansion of calandria tube and thermal contraction of the pressure tube cause the conductance to rapidly decrease.

Acknowledgements

I believe that there is something to learn from every person one meets in life. In that respect, I have to thank all of my family as well as the friends and colleagues that I have been fortunate enough to know for leading me to this accomplishment.

Most importantly, I would like to thank my supervisor, Dr. John Luxat. He allowed me the freedom to approach problems in my own way but guided me in the right direction when I was unsure. His experience and knowledge are unsurpassed. I would also like to thank Dr. David Novog for his advanced thermalhydraulics course. The skills I learned were critical in the completion of my thesis.

My mother and father are the main reason I have made it this far. They have supported me and always believed in me, even when I didn't. Thank you for always answering my questions when I was young, even if you didn't know the answer.

The students in 327 were always a great help and inspiration to me during my time at McMaster; Ken, Dan, Fang, Ricardo, Azin, Farshad, and Hummel. I learned more than was imaginable through discussions about all things science and some not. A simple question would often turn into hours of debate, information exchange and every once in a while an impromptu physics lesson.

Notation and Abbreviations

A	Area
c_{ppt}, c_{pct}	Specific heat of PT and CT
D_{ct}, D_{pt}	Inner diameter of PT and CT
E	Young's modulus
H	Material hardness of the softer material (MPa)
h, h_c, h_g	Thermal contact conductance; Total, solid contact, gas gap regions
h'_{eff}	Effective contact conductance per unit length
h'_{conv}	Boiling convective heat transfer coefficient per unit length
k_s, k_g	Thermal conductivity of solid material and annulus gas
m, m_1, m_2	RMS mean asperity slope, asperity slope of each surface
m'_{pt}, m'_{ct}	Mass of PT and CT per unit length
P, P_g, P_{pt}, P_{ext}	Pressure; contact, annulus gas, internal PT, external CT
q'_{pt}	PT incident heat flux per unit length
R, R_c, R_g	Thermal contact resistance; Total, solid contact, gas gap regions ($R = 1/h$)
r_{pt}, r_{ct}	Radius of PT and CT
T_{pt}, T_{ct}	Temperature of PT and CT
W	Sensitivity function
Y	Mean plane separation

Greek

α_a, $\alpha_{1,\,2}$	Accomodation parameter, coefficients for each surface
β	Fluid parameter
$\dot{\epsilon_{pt}}$, $\dot{\epsilon_{ct}}$	Creep strain rate of PT and CT
$\dot{\epsilon_d}$, $\dot{\epsilon_{gb}}$	Creep strain rate for dislocation creep and grain boundary regions
ϵ_1, ϵ_2	Emissivity of PT and CT surfaces
γ	Ratio of specific heats for annulus gas
Λ, Λ_0	Mean free path and reference mean free path
μ	Ratio of molecular weights of two contacting gas/solid
θ	Mean asperity angle ($m = \|tan\,\theta\|$)
σ	Mean surface roughness
σ_{pt}, σ_{ct}	Azimuthal stress in PT and CT
σ_1, σ_2	Surface roughness of surface 1 and 2
σ_b	Stefan-Boltzmann constant
τ_{pt}, τ_{ct}	Thickness of PT and CT

Abbreviations

CANDU	CANada Deuterium Uranium
CHF	Critical Heat Flux
CHTC	Contact Heat Transfer Coefficient
CT	Calandria Tube
HTC	Heat Transfer Coefficient
LOCA	Loss Of Coolant Accident
PT	Pressure Tube
TCC	Thermal Contact Conductance

Contents

Abstract iv

Acknowledgements vi

Notation and Abbreviations vii

1 Introduction and Problem Statement 1

2 Literature Review 9

2.1 Existing Thermal Contact Conductance Models . . . 9

2.1.1 Ross and Stoute . . . 9

2.1.2 Shlykov and Ganin . . . 10

2.1.3 Cooper et al. . . . 11

2.1.4 Mikic . . . 13

2.1.5 Ainscough . . . 16

2.1.6 Yovanovich . . . 17

2.1.7 Bahrami . . . 21

2.2 Strain in Pressure Tubes and Calandria Tubes . . . 21

2.2.1 Shewfelt Creep Strain Model 21

2.2.2 Fong and Chow 23

2.3 Previous work in PT-CT Contact Conductance 24

2.3.1 Mochizuki and Quaiyum 24

2.3.2 Fan et al. 24

3 Developing a Mechanistic Model 26

3.1 Thermal Contact Conductance Module 27

3.1.1 The Correction Term 31

3.1.2 Surface Hardness 35

3.1.3 Annulus Gas Thermal Conductivity 36

3.1.4 Radiation Heat Transfer 36

3.2 Temperature Module 37

3.2.1 Numerical Solution for the Temperature Equations 39

3.3 Creep Strain Module 40

3.4 Code Assembly 49

4 Results and Analysis 51

4.1 General Code Results and Behaviour 51

4.2 Sensitivity Analysis of Key Parameters 57

4.2.1 Sensitivity of TCC to CT-Moderator HTC 61

4.3 The Effect of Surface Roughness and Asperity Slope 64

4.4 Contact Pressure Results 66

4.5 Treatment of Experimental Data 67

4.5.1 PT Incident Heat Flux Boundary Condition 69

4.6 Comparison to Contact Boiling Tests 70

4.6.1 Comparison to Extracted Data 70

4.6.2 Comparison to Data from Fan et al. 73

4.6.3 Discussion of Results 77

5 Conclusions and Recommendations 80

A Time Step Analysis 87

B TCC Model Development 89

B.1 Solid Conductance 89

B.2 Gas Gap Conductance 91

C Contact Boiling Test Dryout Maps 92

D MATLAB code 94

List of Figures

1.1 Generalized CANDU heat transport system layout [Source: OPG (2001)] 2

1.2 Cut away diagram of CANDU core [Source: Luxat (2009)] 3

1.3 CANDU fuel channel schematic [Source: OPG (2001)] 4

1.4 Fuel channels with normal, sagging and ballooning PTs [Source: Luxat (2009)] 6

1.5 (M.G. Cooper, 1969) Example diagram of microscopic regions of solid contact and gaps in two contacting surfaces 8

2.1 One contact point in a vacuum 12

2.2 Contact conductance as a function of pressure in a vacuum 13

2.3 Diagram from Mikic (1974) illustrating elastic and plastic deformation 15

2.4 Diagram from Mikic (1974) illustrating effect of elastic deformation . 15

2.5 Figure from Ainscough (1982) illustrating effect of gas gap conduction 18

3.1 The PT/CT contact conductance circle of dependency 27

3.2 Solid and gas gap conductance values from Yovanovich model as a function of contact pressure 30

3.3 Accommodation coefficient for zircaloy-CO_2 interface as a function of surface temperature 32

3.4 Accommodation parameter as a function of PT temperature with constant CT temperature . . . 33
3.5 Correction term as a function of PT temperature with constant CT temperature . . . 34
3.6 Heat transfer variables for CT in contact with PT . . . 38
3.7 PT creep strain rate as a function of temperature with internal pressure of 4 MPa . . . 42
3.8 CT dislocation, grain boundary and total creep strain rates as a function of temperature with inter facial pressure of 4 MPa . . . 45
3.9 Flow chart illustrating structure of the creep strain module . . . 47
3.10 Normalized contact pressure vs time for estimated contact pressure ramp-up . . . 48
3.11 Flow chart illustrating overall code structure . . . 50
4.1 TCC and temperature transients for high CT-moderator heat flux . . 53
4.2 TCC and temperature transients for low CT-moderator heat flux . . 54
4.3 Calculated stress transient for CT and PT . . . 55
4.4 Calculated creep strain transient for CT and PT . . . 56
4.5 Dynamic sensitivity of solid contact and gas gap conductance, Functions W1 and W2, to mean surface roughness . . . 59
4.6 Dynamic sensitivity of solid contact and gas gap conductance, Functions W3 and W4, to the ratio of contact pressure and surface hardness 60
4.7 Dynamic sensitivity of PT-CT thermal contact conductance to CT-moderator heat transfer coefficient . . . 62

4.8 TCC transient for varying surface asperity slope to surface roughness ratio 65
4.9 Model prediction for pressure redistribution factor as a function of redistribution factor from Luxat (2002) 66
4.10 Example cross section of contact boiling experiment apparatus (Neal and Fraser, 2003a) 68
4.11 Depiction of thermocouple locations for contact boiling experiment (Neal and Fraser, 2003a) 69
4.12 Comparison of model predictions to extracted CHTC data from ring 4 of experiment SUBC5 72
4.13 Calculated heat fluxes for PT-CT contact transient test SUBC5 . . . 73
4.14 Comparison of model predictions (solid blue line) to data extracted by H.Z. Fan (2004) from experiment Q6 75
A.1 Comparison of CHTC transients obtained from model using different time steps 88
C.2 Dryout map for test SUBC5 (Neal and Fraser, 2003b) with locations of thermocouples circled 93
C.3 Dryout map for test Q6 (H.Z. Fan, 2004) with location of thermocouple 2-90 labeled 93

Chapter 1

Introduction and Problem Statement

The CANada Deuterium Uranium (CANDU) nuclear reactor is a pressure tube-type pressurized heavy water reactor. Diagrams of the heat transport system and core layout are shown in figures 1.1 and 1.2. The core consists of several hundred horizontally oriented fuel channels surrounded by a heavy water moderator and contained in a cylindrical calandria vessel. Each fuel channel has a pressure tube (PT) designed to hold both the fuel bundles as well as pressurized heavy water coolant. Pressure tubes are made of Zr-2.5 wt% Nb and are enclosed within a Zr-2 calandria tube (CT). There is a gap between the PT and CT which is filled with a carbon dioxide annulus gas. Fuel channel design is meant to insulate the fuel and coolant within the PT from the CT in order to prevent high heat losses to the moderator during normal operation. A fuel channel diagram can be seen in figure 1.3.

Under certain types of accident conditions, the moderator may act as a large heat sink which enhances passive safety. In these situations it is desirable to have an

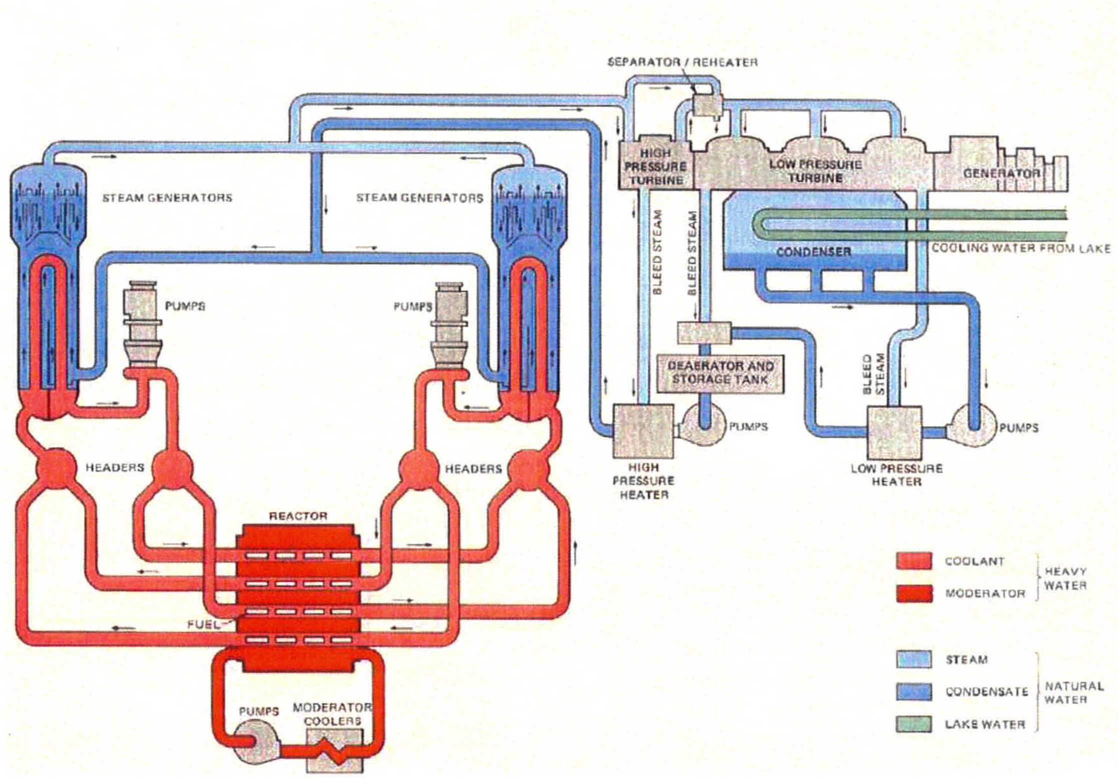

Figure 1.1: Generalized CANDU heat transport system layout [Source: OPG (2001)]

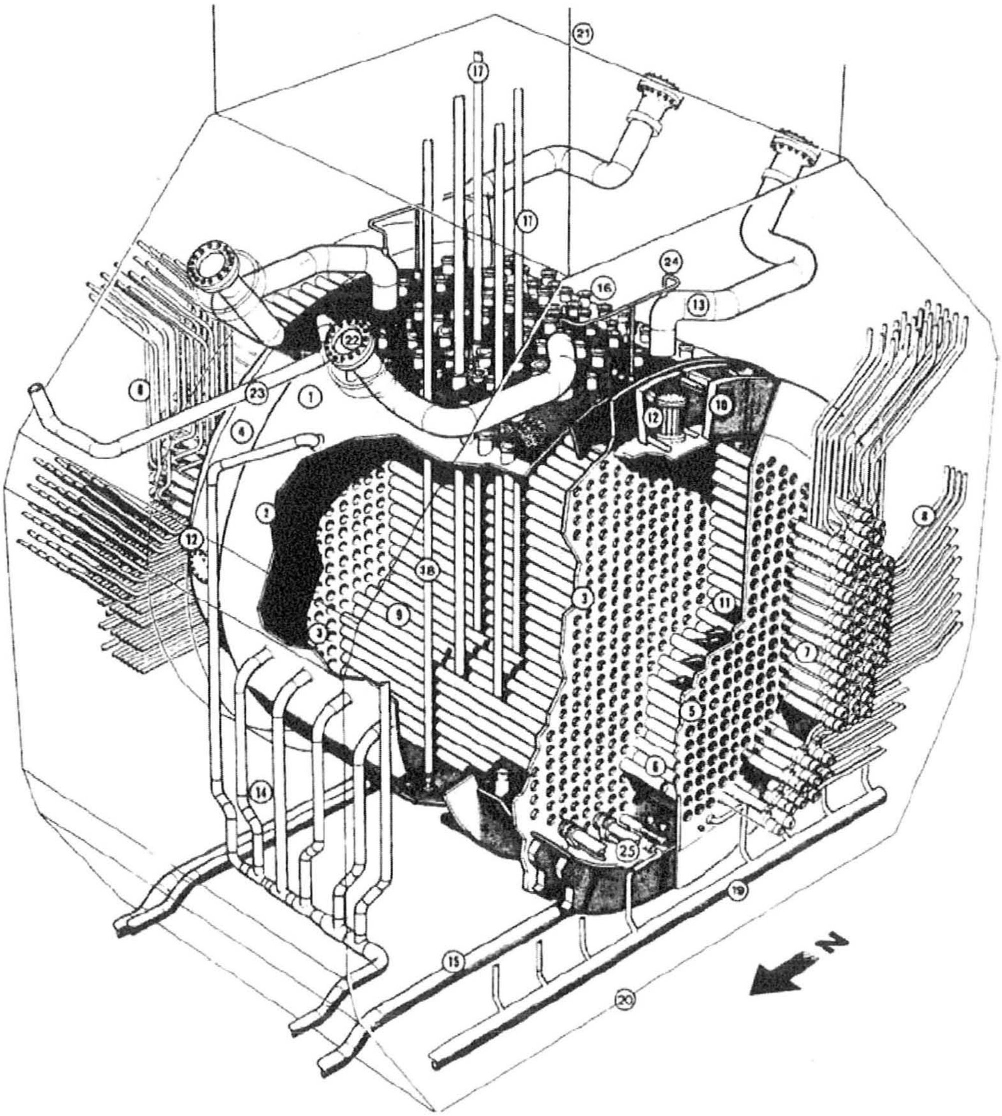

Figure 1.2: Cut away diagram of CANDU core [Source: Luxat (2009)]

established heat transfer pathway from the fuel to the moderator in order to limit fuel channel temperatures and ultimately preserve fuel channel integrity. One such scenario is a Loss Of Coolant Accident (LOCA) where a pipe break in the primary side coolant system leads to loss of coolant inventory and possible loss of normal cooling of the fuel. The worst case is know as a 'critical break' LOCA, where the postulated break is the right size as to cause very low coolant flow in some of the channels in the affected pass. Very low coolant flow leads to rapid overheating of the fuel and pressure tube assembly.

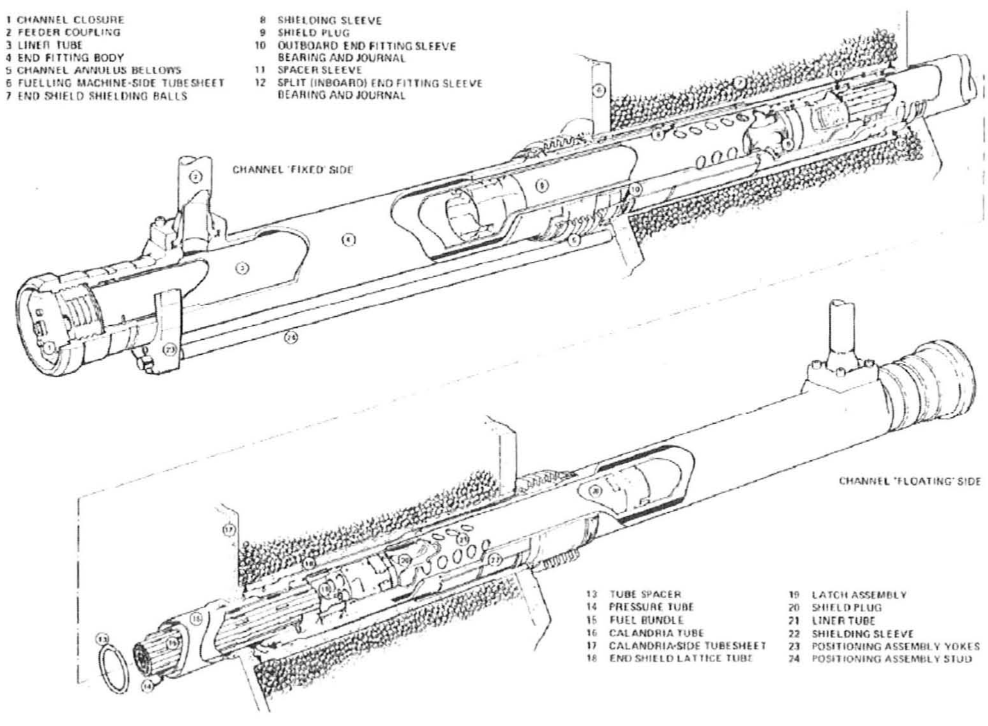

Figure 1.3: CANDU fuel channel schematic [Source: OPG (2001)]

When PT temperatures rise high enough, the PT will start to deform. If the fuel channel is not pressurized, the PT will sag due to gravity and contact the bottom of the calandria tube. If the fuel channel is still pressurized when it starts to deform, it will 'balloon' into contact with the CT resulting in a circumferential contact around the entire PT/CT interface. The latter is the type of deformation studied in this report. A diagram of the two different deformation modes can be seen in figure 1.4.

It is desirable to have a limited value of Thermal Contact Conductance (TCC) between PT and CT. Although an established heat transfer pathway is needed to utilize the moderator as a heat sink, a large heat flux could cause film boiling, or dryout, to occur on the outside surface of the calandria tube. Dryout occurs when the heat flux at a solid-liquid interface exceeds the Critical Heat Flux (CHF). Vapour is formed on the CT outer surface at such a rapid rate that the surrounding liquid cannot wet the surface, causing a degradation of heat transfer. Dryout conditions would severely limit the heat transfer pathway to the moderator and cause further overheating of the fuel channel assembly possibly leading to fuel channel failure.

TCC between pressure tube and calandria tube must be understood as it is a key factor in studying fuel channel integrity. Common practice when performing accident analysis in the past has been to use a constant value of PT-CT TCC as an approximation. In reality, values change quickly with time. The purpose of this investigation is to develop a mechanistic model for representing the TCC transient between pressure tube and calandria tube during a PT ballooning event. The mechanistic model was developed and implemented in a MATLAB code utilizing proven equations and correlations.

A transient PT-CT contact event has several distinct phases as outlined in table 1.1. In the pre-contact phase the pressure tube heats up and deforms with limited heat transfer to the calandria tube. Thus, CT temperatures remain close to the

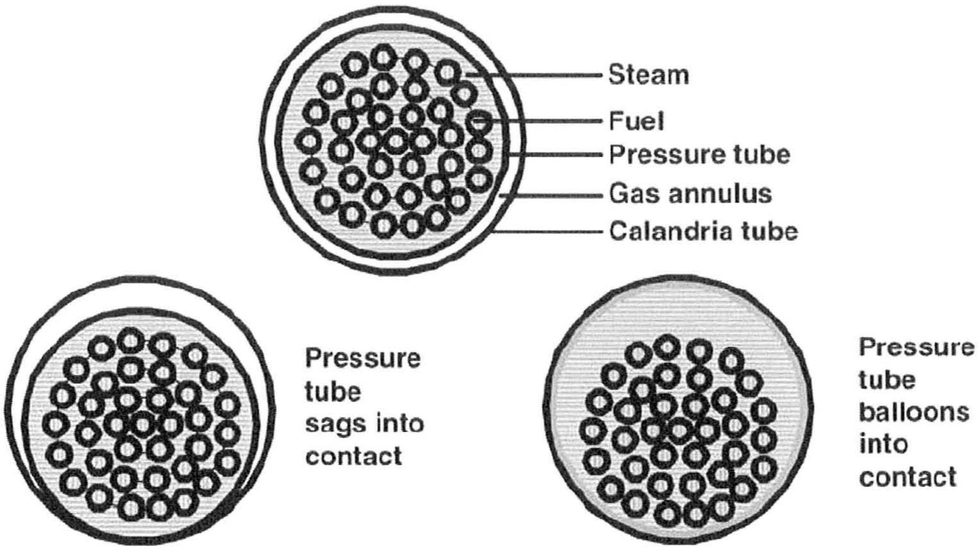

Figure 1.4: Fuel channels with normal, sagging and ballooning PTs [Source: Luxat (2009)]

bulk fluid temperature of the moderator. The initial contact phase includes the instant of contact and ends when the CT starts to deform resulting in decreased interfacial pressure. During this phase contact pressure increases very rapidly to a value approximately equal to the PT internal pressure. In the post-contact phase CT thermal expansion begins due to a high initial heat flux to the CT. As CT temperature rises causing thermal creep and expansion in the CT, the PT temperature drops, causing thermal contraction of the PT. This leads to a drop in contact pressure resulting in TCC leveling off to a constant value lower than the maximum value in the initial contact phase.

Table 1.1: Event sequence and characteristics

Phase	Characteristics
Pre-Contact	• PT heatup • PT creep strain/ballooning • Small amount of conduction/radiation through annulus gas
Initial Contact	• Hard contact pressure • High TCC/heat flux • PT temp drops rapidly • CT temp increases rapidly • Boiling heat transfer/possible dryout on CT external surface
Post-Contact	• PT temp. decreases & levels off • CT temp decreases & levels off • Contact pressure decreases & levels off • TCC decreases & levels off

When two surfaces of differing temperatures come into contact with one another, analyzing the heat transfer between them is not as straightforward as it may seem. All real surfaces, no matter how they are manufactured, have a microscopically rough surface. Surface roughness prevents perfect contact from occurring when two surfaces touch each other. As a result, microscopic contact and gap areas as formed as seen in figure 1.5. Heat transfer modes are different for solid contact areas and gap areas where an interstitial gas may be present. Key parameters that influence conductance values include surface roughness and contact pressure. Many different models and correlations have been developed for both specific and general cases. Chapter two contains a review of some of these models.

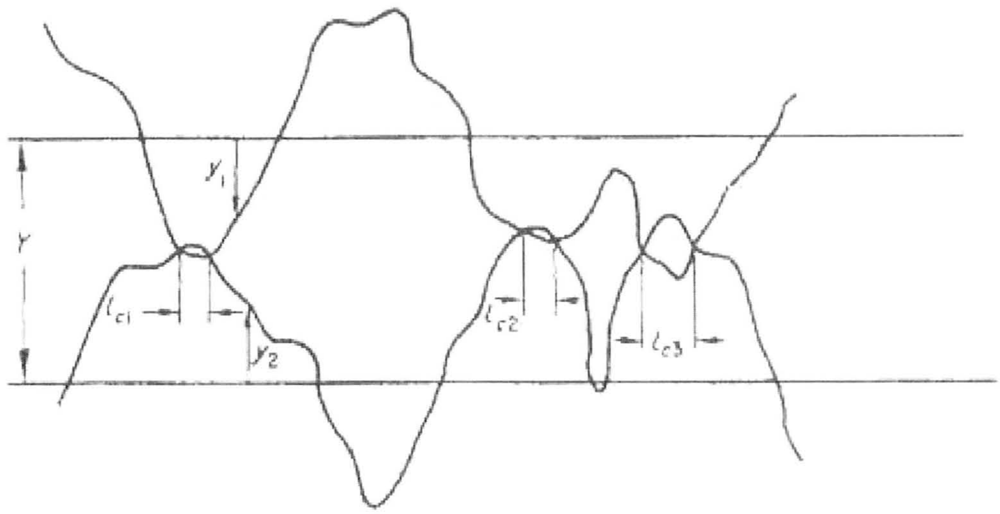

Figure 1.5: (M.G. Cooper, 1969) Example diagram of microscopic regions of solid contact and gaps in two contacting surfaces

This report includes a literature review of relevant material, a chapter on mechanistic model development and an analysis of code results including comparison to several sets of data from contact boiling experiments. It is shown that the method outlined in this report is effective in predicting PT-CT contact conductance transient characteristics for a PT ballooning event.

Chapter 2

Literature Review

2.1 Existing Thermal Contact Conductance Models

A number of different models for thermal contact conductance are available in literature. These models are critically reviewed in the following section.

2.1.1 Ross and Stoute

The Ross-Stoute model (Ross and Stoute, 1962) was developed for contact conductance between fuel pellet and sheath. It is one of the most widely used models in nuclear fuel computer codes. The total conductance is given as the sum of the conductance across contact points, h_c, and the conductance across the gas gap, h_g.

$$h = h_c + h_g \tag{2.1}$$

The conductances of the contact and gap areas are given by the following relationships:

$$h_c = \frac{k_s P_c}{C\sqrt{\sigma^*}H} \tag{2.2}$$

Where, $\sigma^* = \sigma_1^2 + \sigma_2^2$

$$h_g = \frac{2k_g}{\sigma_1 + \sigma_2} \tag{2.3}$$

The solid conductance term is a function of conductivity, surface roughness, surface hardness, contact pressure and an empirical constant. In most solid conductance equations, the most important factor is the ratio of the contact pressure to the hardness of the material. This is because this ratio gives a good indication of the total solid contact area. Due to a fairly simple gas gap conductance term, the Ross-Stoute model is accurate only for high contact pressures such as would occur in a fuel-sheath environment, where the contact pressure is approximately 10 MPa. The gas gap conductance term consists of the interstitial gas thermal conductivity divided by the sum of the effective roughness of each material. In this case, the effective roughness is used as a measure of the mean plane separation between the two surfaces.

2.1.2 Shlykov and Ganin

The Shlykov-Ganin model (Shlykov and Ganin, 1964) is developed under the assumption that the thermal resistances between the contact areas and gas gap areas can be summed like parallel resistors:

$$\frac{1}{R} = \frac{1}{R_c} + \frac{1}{R_g} \tag{2.4}$$

Note that thermal conductivity is the inverse of thermal resistance. This equation is the the same as equation 2.1. Thermal resistance across the gas gap is treated in a similar way to the Ross-Stoute model. It is assumed that there is no convection, therefore the conductance through the gap is modeled using the gas conductivity and a gas gap thickness estimate based on the material roughness.

The contact resistance is developed assuming that each contact point has the same area. Increasing the contact pressure only increases the number of contact points and not the individual contact area. Resistances of each contact site are summed as parallel resistances. This gives the relationship:

$$R_c = \frac{3\sigma_b S}{2.1 N \lambda_m} \times 10^{-4} \tag{2.5}$$

Where;

σ_b, is the ultimate material strength

λ_m, is the thermal conductance of the material

N, is the normal surface loading

S, is the nominal contact area

2.1.3 Cooper et al.

Cooper, Mikic and Yovanovich perform an analysis of heat transfer on the basis of one contact location between two thick materials in a vacuum. The idea is then expanded to include the scenario of multiple contact locations which is more applicable to real world problems. Figure 2.1, from M.G. Cooper (1969), shows a visualization of the one contact point model with a corresponding plot of the temperature profile across the gap. For the 'appropriately' distributed model of multiple contacts outlined, it

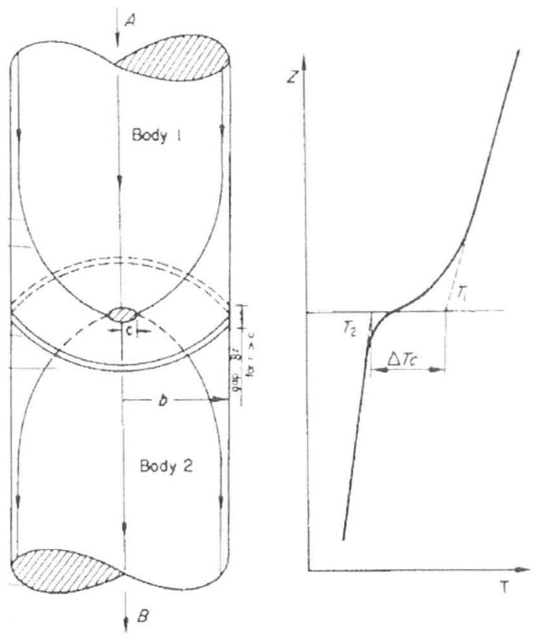

FIG. 1. Elemental flow channel; definition of ΔT_c.

Figure 2.1: One contact point in a vacuum

is assumed that for each contact point the heat flow takes the shape of a straight cylindrical flow channel. It is also assumed that the temperatures at each contact point are the same which is reminiscent of an electrical analogy using parallel resistors. The height of the surface asperities were assumed to have a Gaussian distribution which led to the following expression;

$$\frac{h_c}{k_s}\frac{\sigma}{||\tan\theta|} = \left[\frac{P}{H}\right]^{0.985} \tag{2.6}$$

Cooper et al. published a plot of this equation with experimental data as seen in figure 2.2 for known values of h_c and σ determined by a profilometer trace. The predicted values fall approximately 50% above that in experimental data. This is an acceptable range for most contact conductance models.

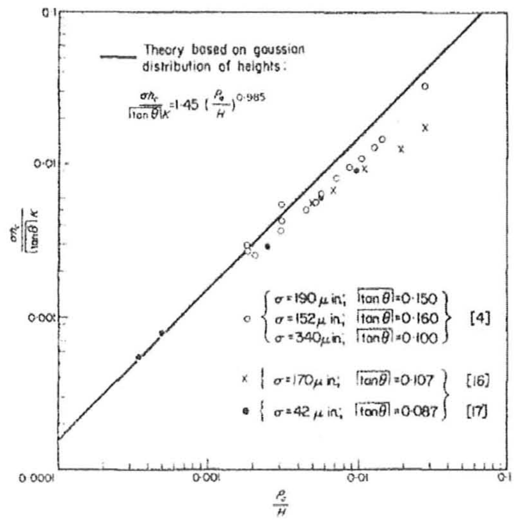

Figure 2.2: Contact conductance as a function of pressure in a vacuum

2.1.4 Mikic

Mikic performed an extensive review of contact conductance models developed up to 1974 with a focus on surface behavior. Two main modes of interaction between nominally flat surfaces are presented; plastic deformation and elastic deformation. In plastic deformation, three models are reviewed; the geometric model, a model which considers plastic flow of material and a model with correction for elastic displacement. The geometric model uses the simplifying idea of one rough surface interacting with a flat surface. It is assumed that bringing the two surfaces together within a distance Y is equivalent to slicing off the top of the asperities at a height Y above the mean plane of interaction. The fraction of area in contact compared to total are is given as:

$$A = 0.5erfc\left(\frac{\eta}{\sqrt{2}}\right) \equiv Q(\eta) \tag{2.7}$$

$$\eta \equiv \frac{Y}{\sigma} \tag{2.8}$$

Where σ is the standard deviation of profile height for the rough surface. This leads to an approximation for contact conductance due to plastic deformation:

$$\overline{h_p} = 1.13\frac{k\tan\theta}{\sigma}\left(\frac{P}{H}\right)^{0.94} \tag{2.9}$$

This expression does not take into account plastic flow of material. It is noted that for large contact pressure where the maximum fraction of contact area that can be reached is one half of the total area. This cannot be true as plastic deformation will cause a uniform rise over the entire surface. A modified version of the above equation takes into account plastic relocation of material:

$$\overline{h_p} = 1.13\frac{k\tan\theta}{\sigma}\left(\frac{P}{H+P}\right)^{0.94} \tag{2.10}$$

This modification will tend to reduce the contact conductance at large loads while approximating the non-plastic flow model. Another correction can be made if we take into account elastic displacement of the substrate under the contact points. A diagram illustrating this is shown in figure 2.3. This modification has the effect of reducing the contact area as can be seen in figure 2.4. A_0 is the contact area from plastic deformation alone and A is the contact area using the elastic deformation of substrate model. For the case of elastic deformation, contact area can be related to the displacement using Hertzian theory. Mikic has shown that for the same separation

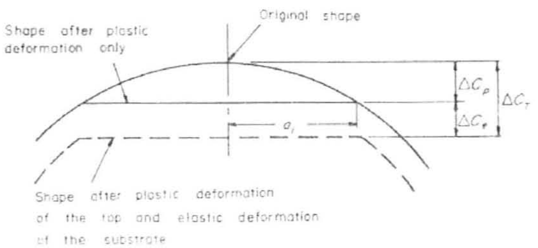

FIG. A1. An asperity in plastic deformation with elastic deformation of the substrate.

Figure 2.3: Diagram from Mikic (1974) illustrating elastic and plastic deformation

Thermal contact conductance

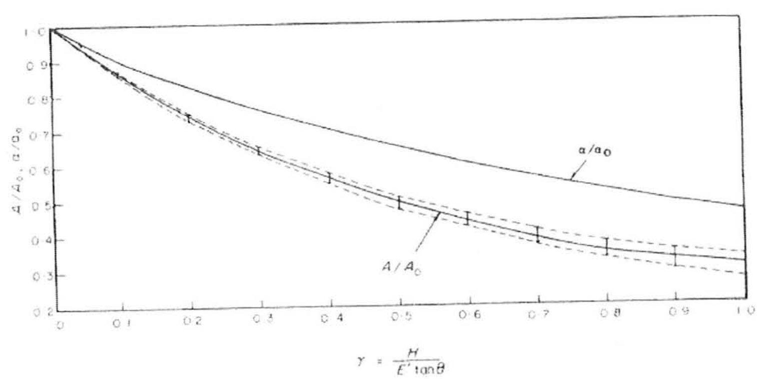

FIG. 3. Effect of elastic deformation of substrate on contact parameters.

Figure 2.4: Diagram from Mikic (1974) illustrating effect of elastic deformation

between contacting surfaces, the contact area for the plastic deformation model will equal twice the contact area of the elastic deformation model. The equation for contact conductance using the elastic deformation model is:

$$\overline{h_e} = 1.55\frac{k\tan\theta}{\sigma}\left(\frac{P\sqrt{2}}{E\tan\theta}\right)^{0.94} \quad (2.11)$$

When plastic contact pressure and elastic contact pressure are equal it does not imply that the interface pressures are the same, as both are uniquely defined;

$$P_e = \frac{\sqrt{2}P}{E\tan\theta} \quad (2.12)$$

$$P_p = \frac{P}{H} \quad (2.13)$$

2.1.5 Ainscough

The Ainscough report was prepared under the auspices of the OECD Nuclear Energy Agency and is a review of current fuel cladding gap conductance methods used for light water reactors up to 1982. The governing equations for heat transfer from fuel to cladding are given with common assumptions used in modeling codes. The gap conductance is broken down in a similar fashion to that employed by Ross and Stoute except with an additional term for radiative heat transfer. However, in most cases heat transfer by radiation is negligible and only has an effect at high temperatures.

Ainscough explains that most codes make an incorrect assumption in treating the gas portion of the gap as open. Since most LWR fuel-cladding gaps are very small, a different form of the equation is required:

$$h_g = \frac{k_g}{d + d_{min} + g_f + g_c} \tag{2.14}$$

Where;

k_g, is the thermal conductivity of the gas in the gas gap

d, is the open gap width

d_{min}, is a term related to the roughness of the surfaces

g_f and g_c, are temperature jump distance extrapolations which account for discontinuities in energy exchange between gas and surface

The solid conductance model presented is of a common form described by Ross and Stoute, where the surface roughness parameter is defined by the root mean square roughness of both surfaces. An alternate definition by Hobbs, defines the roughness parameter as the square root of the sum of both roughness values. Figure 2.5, above, illustrates the effect of conduction through the solid contact point and through the gas gap as opposed to just solid conduction alone. The lines in the diagram are isothermal planes emanating from the contact point. This emphasizes the fact that we must understand conduction through the gas gap in conjunction with solid contact conductance.

2.1.6 Yovanovich

By further development of the equations by Cooper and Mikic, Yovanovich produces the following equations for solid and gas gap conductance (Yovanovich, 1981). One of the key aspects of this model is the introduction of a new equation for calculating

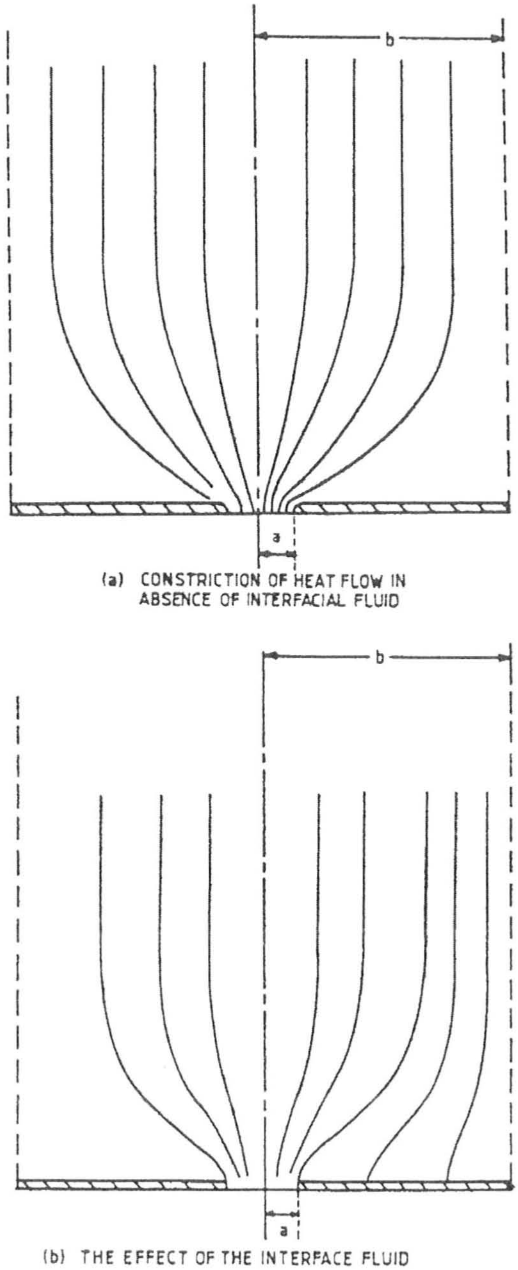

Figure 2.5: Figure from Ainscough (1982) illustrating effect of gas gap conduction

the heat transfer coefficient through the gas gap. In Equation 2.16 the gas gap conductance is inversely proportional to the mean plane separation plus other factors including accommodation parameter, mean free path, and a fluid parameter.

$$h_c = 1.25\frac{k_s m}{\sigma}\left(\frac{P}{H}\right)^{0.95} \tag{2.15}$$

$$h_g = \frac{k_s}{Y + \alpha_a \beta \Lambda} \tag{2.16}$$

$$Y = 1.184\sigma\left[-ln\left(\frac{3.132P}{H}\right)\right]^{0.547} \tag{2.17}$$

Equation 2.17 for mean plane separation is an approximation for the inverse error function. This is a result of the statistical nature of the surface asperities. As in M.G. Cooper (1969) it is assumed that surface feature values form a Gaussian distribution. Mean plane separation is dependent on P/H ratio as well as surface roughness. Equation 2.18 for the mean free path is calculated using a reference mean free path, temperature and pressure in conjunction with the pressure and temperature of the gas gap. Equation 2.19 is the fluid parameter, which is dependent on the gas gap specific heat ratio and Prandtl number.

$$\Lambda = \Lambda_0\left(\frac{T_m}{T_{m0}}\right)\left(\frac{P_{g0}}{P_g}\right) \tag{2.18}$$

$$\beta = \left(\frac{2\gamma}{\gamma+1}\right)\frac{1}{Pr} \tag{2.19}$$

$$\alpha_a = \frac{2-\alpha_1}{\alpha_1} + \frac{2-\alpha_2}{\alpha_2} \tag{2.20}$$

The accommodation parameter α_a is used to correct for interaction between the gas and solid by determining the kinetic energy exchanges in a collision of a gas molecule with the solid wall. Accommodation coefficients α_1 and α_2 are determined empirically for different gas/solid combinations and is sensitive to the condition of the solid surface. In a paper by Bahrami and Yovanovich (M. Bahrami, 2004a), a correlation for the accommodation coefficients is given.

$$\alpha = exp\left[-0.57\left(\frac{T_s - T_0}{T_0}\right)\right]\left(\frac{M_g^*}{6.8 + M_g^*}\right) + \frac{2.4\mu}{(1+\mu)^2}\left\{1 - exp\left[-0.57\left(\frac{T_s - T_0}{T_0}\right)\right]\right\} \tag{2.21}$$

Where $T_0 = 273K$, $M_g^* = M_g$ for monatomic gases and $M_g^* = 1.4M_g$ for diatomic and polyatomic gases.

Lemczyk and Yovanovich (1987) compared the preceding methods against data and developed an iterative algorithm for contact conductance in compound tubes using the above equations. The algorithm involves iterating with a guessed contact pressure to calculate contact conductance. The calculated conductance is used to determine radial stress in the inner and outer sections of the compound cylinder. A new contact pressure is determined and the procedure is repeated until convergence. This work shows that the Yovanovich correlations for gap conductance are an improvement over older correlations and are valid for the case of compound cylinders such as in pressure tube-calandria tube contact conductance.

2.1.7 Bahrami

M. Bahrami (2004b) use a scale analysis method to predict thermal contact resistance. A non-dimensional parameter is introduced to help classify three types of contact resistance. The new parameter is defined as the ratio of macrothermal to microthermal resistance. The three types of contact resistance are defined as; conforming rough, elastoconstriction and transition region. In the conforming rough region, the two surfaces have relatively low curvature and microthermal resistance is the dominant effect. Micro contacts are treated as parallel resistors. In the elastoconstriction regime, the surfaces are relatively smooth and have a small radius of curvature. This causes macrothermal resistance to be the dominant effect.

2.2 Strain in Pressure Tubes and Calandria Tubes

From the contact conductance models described in the previous section, it is apparent that contact pressure is one of the key variables in determining contact conductance between two surfaces. Contact pressure may be determined if we can understand how PT and CT will react to both the forces acting on them and high temperature levels.

2.2.1 Shewfelt Creep Strain Model

Understanding creep strain in zircaloy materials such as pressure tubes and calandria tubes used in CANDU reactors is difficult at higher temperatures. This is because of the phase change which occurs in the zircaloy lattice. Shewfelt et al. developed a creep model for the cold-worked Zr-2.5 wt% Nb material used in CANDU pressure tubes (R.S.W. Shewfelt, 1984). This was accomplished by taking both transverse and longitudinal samples from actual CANDU pressure tubes and testing them in a uniaxial creep apparatus.

$$\dot{\epsilon_{pt}} = 1.3 \times 10^{-5} \sigma_{pt}^{9} exp\left(-36600/T_{pt}\right) + \frac{5.7 \times 10^{7} \sigma_{pt}^{1.8} exp\left(-29200/T_{pt}\right)}{\left[1 + 2 \times 10^{10} \int_{t_1}^{t} exp\left(-29200/T_{pt}\right) dt\right]^{0.42}} \tag{2.22}$$

Equation 2.22 is valid for a temperature range of 450°C to 850°C. It provides the transverse creep strain rate as a function of temperature and stress. The first term represents power law creep in the α-phase, which is the dominant mode up to 500°C. The second term is due to grain boundary sliding which is the dominant mode after 500°C. Above 850°C, different mechanisms of deformation exist due to a mostly β-phase structure. This results in the need for different a different equation for the higher temperature range.

In another paper, Shewfelt developed creep strain rate equations for the Zr-2 material used in calandria tubes (R.S.W. Shewfelt, 1988). Equation 2.24 and 2.26 are the dislocation and grain boundary sliding creep for Zr-2 calandria tubes. The total calandria tube creep strain rate is the sum of these two creep mechanisms.

$$\dot{\epsilon_{ct}} = \dot{\epsilon_{d}} + \dot{\epsilon_{gb}} \tag{2.23}$$

$$\dot{\epsilon_{d}} = 22000 \left(\sigma_{ct} - \sigma_{i}\right)^{5.1} exp\left(-34500/T_{ct}\right) \tag{2.24}$$

$$\sigma_i(t) = 1.4 + \int_0^t \left[110\dot{\epsilon_d} - 3.5 \times 10^{10} \sigma_i^{1.8} exp\left(-34500/T_{tc}\right)\right] dt \tag{2.25}$$

$$\dot{\epsilon_{gb}} = 140 \sigma_{ct}^{1.3} exp\left(-19000/T_{ct}\right) \tag{2.26}$$

Luxat (2002) defines an expression for interfacial pressure between PT and CT.

Contact pressure is a function of PT internal pressure, CT external pressure and a pressure redistribution factor. The redistribution factor, a_{pc}, is calculated assuming that creep rates of the contacting PT and CT are equal. Therefore it depends on the parameters in the Shewfelt equations, namely temperature and stress, and is evaluated iteratively to obtain equality of the two strain rates.

$$P = a_{pc}P_{pt} + (1 - a_{pc})\,P_{ext} \tag{2.27}$$

2.2.2 Fong and Chow

Fong and Chow (2002) conducted work with the intent to address the issue of variability in CANDU pressure tubes. This variability in creep can occur because of differences in chemical composition, manufacturing techniques, or microstructure changes due to irradiation in the reactor core. In the paper, creep strain tests similar to those carried out by Shewfelt, are performed on different pressure tube specimens. The specimens range from unirradiated 'offcut' samples taken from the pressure tube ends, to irradiated samples taken from the in-core portions of the same tubes. Variations are seen between specimens taken from the 'front-end' and 'back-end' of the tubes. The contact temperature (temperature at which strain of 18% is reached) was observed to be higher in offcut samples taken from the front-end. There was no observable trend for the difference between irradiated specimens and unirradiated specimens, however the amount of data was limited.

2.3 Previous work in PT-CT Contact Conductance

2.3.1 Mochizuki and Quaiyum

Mochizuki and Quaiyum (1994) conducted experiments to determine contact conductance pressure tube and calandria tube materials. Experiments were done for varying contact pressure, interstitial gas pressure, and different types of artificial waviness machined into the materials. Results for clean plates as well as plates covered with Fe_2O_3 'simulated crud' were compared. It was found that the presence of crud on PT walls serves to decrease contact conductance.

2.3.2 Fan et al.

Many contact boiling experiments have been conducted in order to determine fuel channel behaviour during a pressure tube deformation event. In these experiments only the heater power and PT and CT temperatures are recorded. Since the PT-CT contact conductance is not directly measured, it must be extracted from the available data. H.Z. Fan (2002) presents a methodology to calculate the transient behaviour of PT-CT contact conductance for these contact boiling experiments. An empirical correlation for contact heat transfer coefficient is given in the form:

$$h_c = Ck\left(K_P P_{channel}\right) + h_0 \tag{2.28}$$

Where C is a material constant, K_P is a dimensionless pressure factor and h_0 is a lumped heat transfer coefficient for gas gap and radiation conductance. A model is derived for use with a thermalhydraulic computer code, using the incident heat flux on the inner surface of the pressure tube and the measured calandria tube temperature as boundary conditions.

Chapter 3

Developing a Mechanistic Model

This chapter will take an in depth look into the three basic modules required for development of a PT/CT thermal contact conductance model. Key parameters and behavior of each module will be investigated and assimilated into the code.

The three modules are:

Thermal Contact Conductance

Creep Strain

Temperature/Heat Equations

Each module has an input and an output directly related to the other modules. Figure 3.1 illustrates the relationship between each module. TCC is dependent on contact pressure which is determined from creep strain equations in both tubes. Creep strain is in turn dependent on the temperature of each tube and TCC plays a major role in tube temperatures.

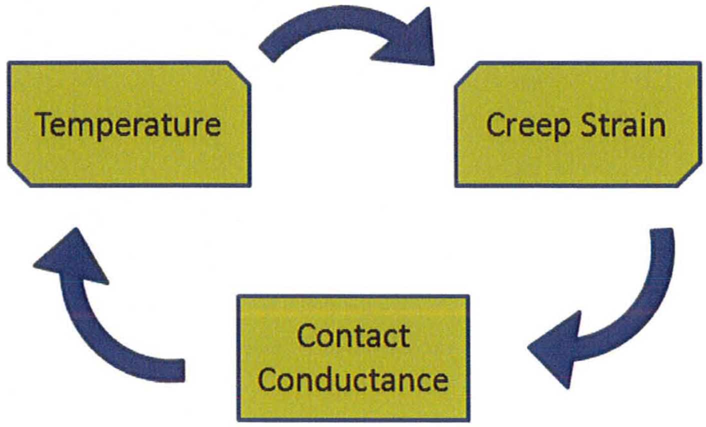

Figure 3.1: The PT/CT contact conductance circle of dependency

The main assumptions made are:

1. Radial creep is uniform in the azimuthal direction
2. There is no strain in the axial direction
3. Once initial contact is made PT and CT creep rates are equal
4. At initial contact, contact pressure increases to its maximum rapidly
5. Radiation heat transfer between PT and CT is negligible

3.1 Thermal Contact Conductance Module

The main function of the TCC module is to receive input from the other modules and calculate the contact conductance. The main input is contact pressure obtained from the creep strain module although some parameters require temperature input. The TCC model developed by Yovanovich (1981) for conforming rough surfaces was selected for the TCC module. It can be seen in section 2.1.6 along with the equations used in the computer code. Selection was based on findings in literature which demonstrate that the Yovanovich correlations give accurate results for the case of concentric cylinders; a similar geometry to PT-CT contact (Lemczyk and Yovanovich, 1987). Also, it was chosen over other models, such as the Ross-Stoute model because of its ability to calculate mean plane separation. This is important because for the contact pressure range in PT-CT contact, solid and gas gap conductivity are of comparable magnitude. Models such as Ross-Stoute, which was developed for the fuel-cladding interface, only provide an estimate using surface roughness values for gap width. This is acceptable for some scenarios where the gas gap conductance is significantly smaller than the solid conductance. When the two are comparable however, a more accurate value for mean plane separation is needed.

There are many key parameters which influence the Yovanovich model for TCC. Most of them are relevant to all contact conductance correlations and are discussed below.

The ratio of contact pressure to surface material hardness, P/H, is a key parameter for determining solid contact area. This is because the total solid conductance is proportional to the total area of the solid contact regions. As inter facial pressure is increased, the contacting surfaces get pressed together with greater force resulting in a higher area of solid contact.

Surface roughness, σ, is also a key parameter. Finer surface finishes (smaller surface asperities), result in higher values of conductance. This is due to roughness effects on mean plane separation, which increases gas gap conductance for a finer surface finish. Also, smaller roughness values result in the presence of more contact points which yield a greater solid contact area.

Mean plane separation, Y, is the main parameter influencing conduction through the gas gap regions. Most TCC models assume that the gas gap area is too small for convective heat transfer; therefore the gas gap conductance is inversely proportional to the mean plane separation of the two surfaces.

Acceptable ranges of parameters for the TCC model as given in Lemczyk and Yovanovich (1987) are presented in table 3.1.

Table 3.1: Acceptable Ranges of Parameters

10^{-5}	$<$	P/H	$<$	10^{-2}
2.34	$<$	Y/σ	$<$	4.26
$0.14\,\mu m$	$<$	σ	$<$	$14\,\mu m$
$9.33\,\mu m$	$<$	σ/m	$<$	$40\,\mu m$
0.015	$<$	m	$<$	0.35
2	$<$	α_a	$<$	420
1	$<$	β	$<$	2
$0.04\,\mu m$	$<$	Λ_o	$<$	$0.19\,\mu m$

Figure 3.2 is a plot of Yovanovich correlations for solid conductance and gas gap conductance as a function of contact pressure. The gas gap (Equation 2.16) term applied does not include the fluid, mean free path, and accommodation parameters as they have dependency on the surface temperatures which will be calculated later. As shown in the plot, the solid contact conductance has an almost linear relationship with respect to contact pressure. The gas gap conductance also increases with contact pressure. This is due to a smaller value of mean plane separation at higher contact pressures.

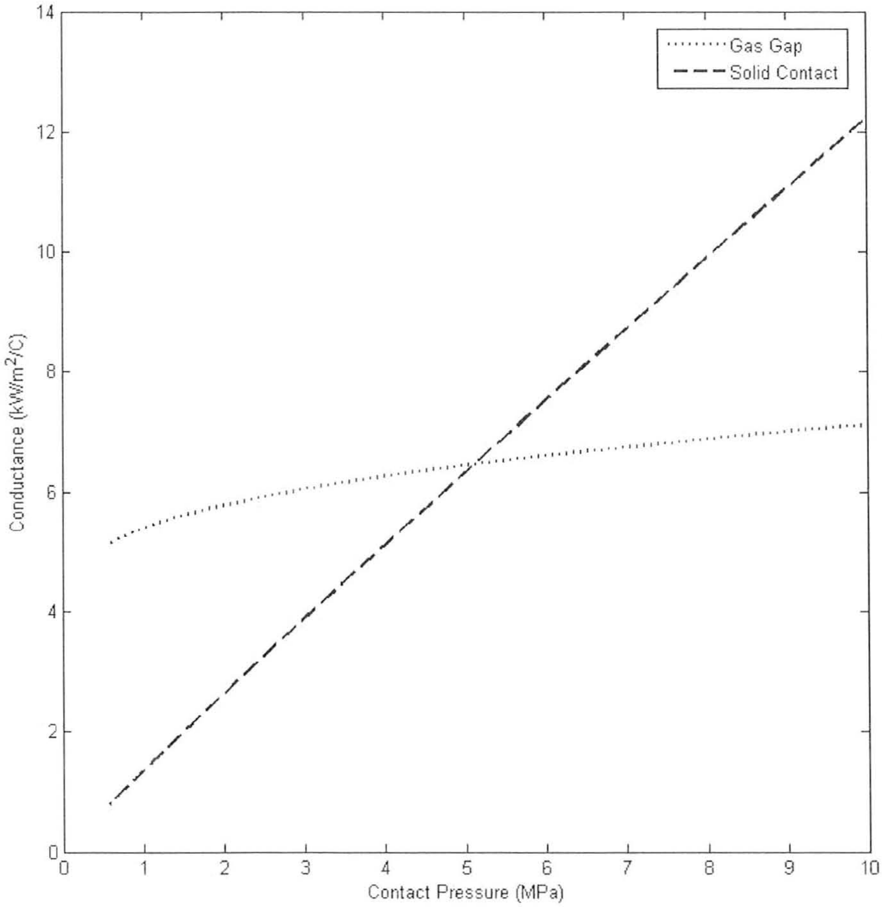

Figure 3.2: Solid and gas gap conductance values from Yovanovich model as a function of contact pressure

3.1.1 The Correction Term

The calculation for mean free path is done using a reference value at a given temperature and pressure. From Equation 2.18 it is seen that mean free path is proportional to temperature and inversely proportional to pressure. In the mechanistic model, it is assumed that the annulus gas pressure remains constant. This is based on the assumption that the gas gap areas formed are not isolated from one another and the annulus gas is allowed to expand as temperature rises. The temperature of the gas in the gas gap will be calculated as the average of PT and CT temperatures. The new equation for mean free path is:

$$\Lambda = \Lambda_0 \left(\frac{T_{PT} + T_{CT}}{2T_{m0}} \right) \tag{3.1}$$

For the carbon dioxide used as the annulus gas the mean free path is $90nm$ at a reference temperature of $500K$ and atmospheric pressure. Mean free path is in units of length and gives the $\alpha_a \beta \Lambda$ correction term units of length as well because both fluid and accommodation parameters are dimensionless. Mean free path is significant in gap conductance because of the microscopic nature of the problem. When the Knudsen number (ratio of molecular mean free path to some characteristic length) approaches unity, it can no longer be assumed that the annulus gas functions as a continuous medium. Molecular interactions with the solid wall are just as likely to occur than collisions between molecules. As the mean free path gets smaller, the $\alpha_a \beta \Lambda$ correction term gets smaller as well which approximates the macroscopic/microscopic behaviour of the system.

Because the Knudsen number is small, the accommodation parameter (Equation

2.20) is important. The correlation for accommodation coefficient shown in Equation 2.21 is plotted as a function of surface temperature for the zircaloy-CO_2 interface in Figure 3.3. Values for accomodation coefficient are approximated at 0.85 in SCDAP/RELAP5 (1997). The results presented here give a value of 0.85 at approximately 350 K for the zircaloy-CO_2 interface. Figure 3.4 shows how the accommodation parameter acts with given accommodation coefficient input by assuming a constant calandria tube temperature.

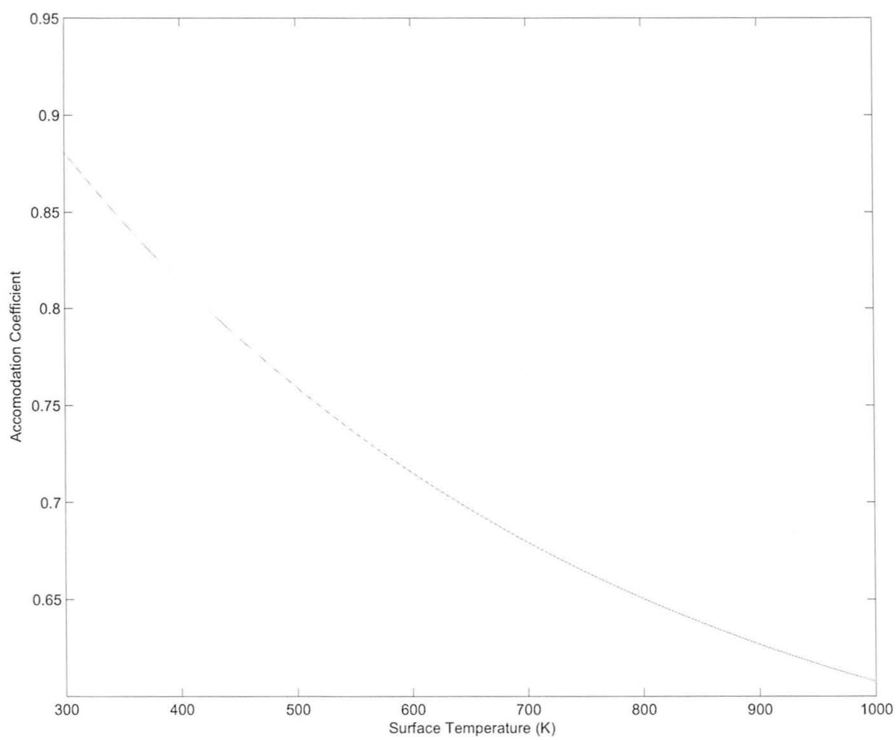

Figure 3.3: Accommodation coefficient for zircaloy-CO_2 interface as a function of surface temperature

The fluid parameter (Equation 2.19) contains the Prandtl number. The Prandtl

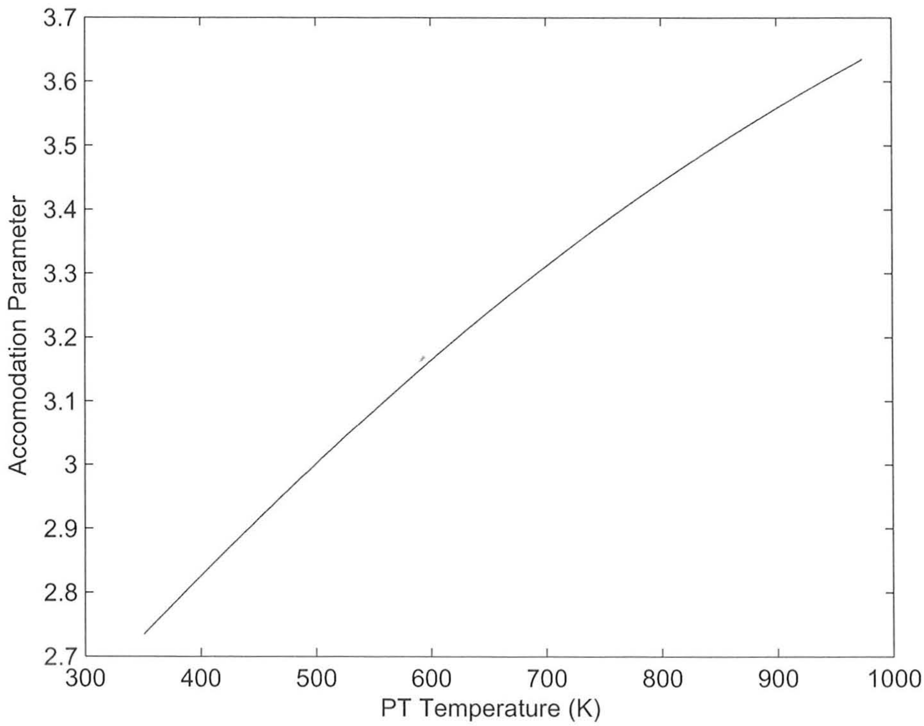

Figure 3.4: Accommodation parameter as a function of PT temperature with constant CT temperature

number gives an indication of which type of heat transfer mode is dominant in a fluid. The fluid parameter increases as the ratio of thermal diffusion to viscous diffusion increases. Figure 3.5 shows the total behaviour of the correction term as a function of pressure tube temperature assuming a constant calandria tube temperature of $350K$. The correction term is roughly two orders of magnitude smaller than the mean plane separation, Y, during the post contact phase.

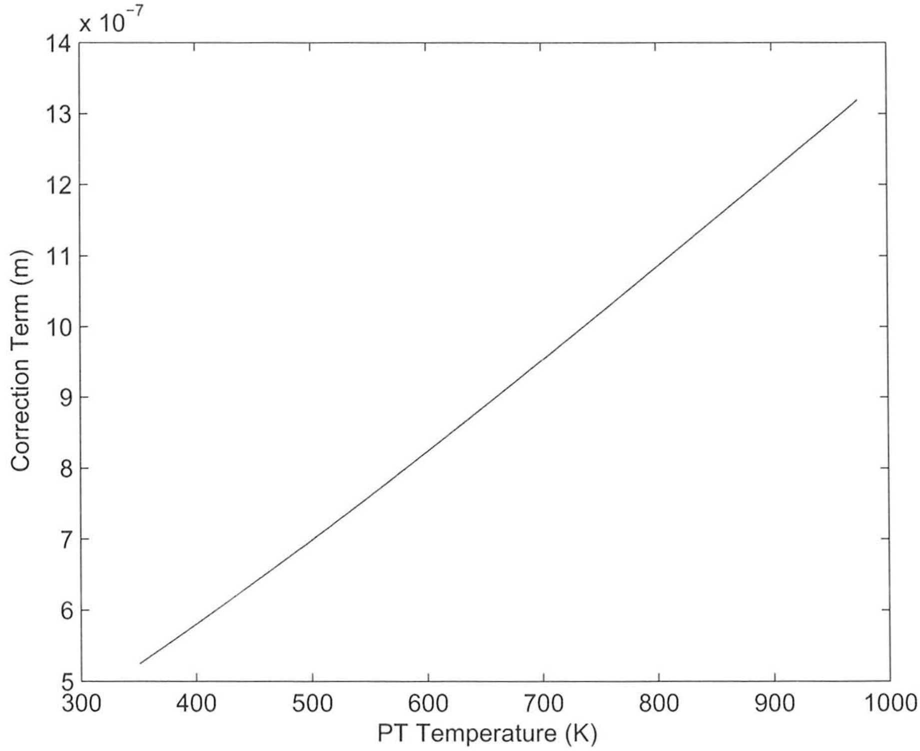

Figure 3.5: Correction term as a function of PT temperature with constant CT temperature

3.1.2 Surface Hardness

Surface hardness is one component of one of the key parameters identified on page 28. The surface hardness of materials usually decreases with temperature. A correlation for the Meyer hardness of zircaloy (SCDAP/RELAP5, 1997) is used to approximate the hardness of the softer surface.

$$H_m = exp[26.034 + T[-2.6394 \times 10^{-2} + T(4.3504 \times 10^{-5} - T2.5621 \times 10^{-8})]] \quad (3.2)$$

Where T is in units of Kelvin and Meyer hardness is in Pa. The value for Meyer hardness of the softer of the two contacting materials is used in most contact conductance correlations.

The Yovanovich model uses contact microhardness for the P/H parameter. Contact microhardness can be calculated if bulk hardness values, such as Meyer hardness, as well as surface roughness and mean asperity slope are known. An iterative model for calculation of contact microhardness is presented in Yovanovich (2006). Studies on the iterative model by Song and Yovanovich (1988) concluded that the results could be expressed by the following equation:

$$\frac{P}{H_c} = \left[\frac{P}{1.62c_1(\sigma \times 10^6/m)^{c_2}}\right]^{1/1+0.071c_2} \quad (3.3)$$

Where H_c is the contact microhardness and c_1 and c_2 are the Vickers correlation coefficient and Vickers size index respectively. The Vickers correlation coefficient can be determined from the following correlation (Yovanovich, 2006) if c_2 and bulk hardness (Meyer hardness) values are known:

$$c_1 = \frac{0.442 H_b}{c_2 + 0.370} \tag{3.4}$$

The Vickers size index, c_2, is given in (Yovanovich, 2006) as -0.267 for Zr-Nb. The bulk hardness value, H_b is taken as the Meyer hardness for this case.

3.1.3 Annulus Gas Thermal Conductivity

Carbon dioxide annulus gas fills the gas gap region between the contacting surfaces. Thermal conductivity of this gas is highly dependent on temperature. A correlation shown below for carbon dioxide (SCDAP/RELAP5, 1997) is applied to calculate thermal conductivity of the gas.

$$k_{co_2} = 9.460 \times 10^{-6} T^{1.312} \tag{3.5}$$

Where temperature is in units of Kelvin and thermal conductivity is in $kW/m{\cdot}K$. The temperature of the gas is approximated as the average of PT and CT temperatures and updated every time step.

3.1.4 Radiation Heat Transfer

During the development of the model it was assumed that radiation heat transfer between the two surfaces is negligible. This assumption was based on a rough calculation for radiation heat transfer. An equation from Incropera and DeWitt (2002) for long concentric cylinders was used (Equation 3.6).

$$q_r = \frac{A\sigma_b\left(T_1^4 - T_2^4\right)}{\frac{1}{\epsilon_1} + \frac{1-\epsilon_2}{\epsilon_2}\left(\frac{r_1}{r_2}\right)} \tag{3.6}$$

Assuming that the radii of the two tubes are equal at contact ($\frac{r_1}{r_2} = 1$) and solving for radiative heat transfer coefficient per unit area;

$$h_r = \frac{q_r}{A\left(T_{PT} - T_{CT}\right)} = \frac{\sigma_b\left(T_{PT}^2 + T_{CT}^2\right)\left(T_{PT} + T_{CT}\right)}{\frac{1}{\epsilon_1} + \frac{1-\epsilon_2}{\epsilon_2}} \tag{3.7}$$

Assuming surface emissivities of 0.8 and 0.3 for PT and CT respectively, the radiative heat transfer coefficient is 28 $W/m^2/K$ which is three orders of magnitude less than the expected contact conductance.

Before PT-CT contact is made, there is still a small amount of heat transfer to the calandria tube due to conduction through the carbon dioxide annulus gas. This is approximated by the following equation;

$$h_g = \frac{k_g}{\eta} \tag{3.8}$$

Where, η is the separation distance between the PT outer surface and CT inner surface.

3.2 Temperature Module

The temperature/heat equations module serves to iteratively compute PT and CT temperatures using a system of lumped parameter heat transfer equations. The main input into the temperature module is the contact conductance which was calculated in the TCC module. In order to understand the heat transfer characteristics of the system Figure 3.6 shows the boundary conditions and other variables present. Boundary conditions are the incident heat flux on the inside of the pressure tube as

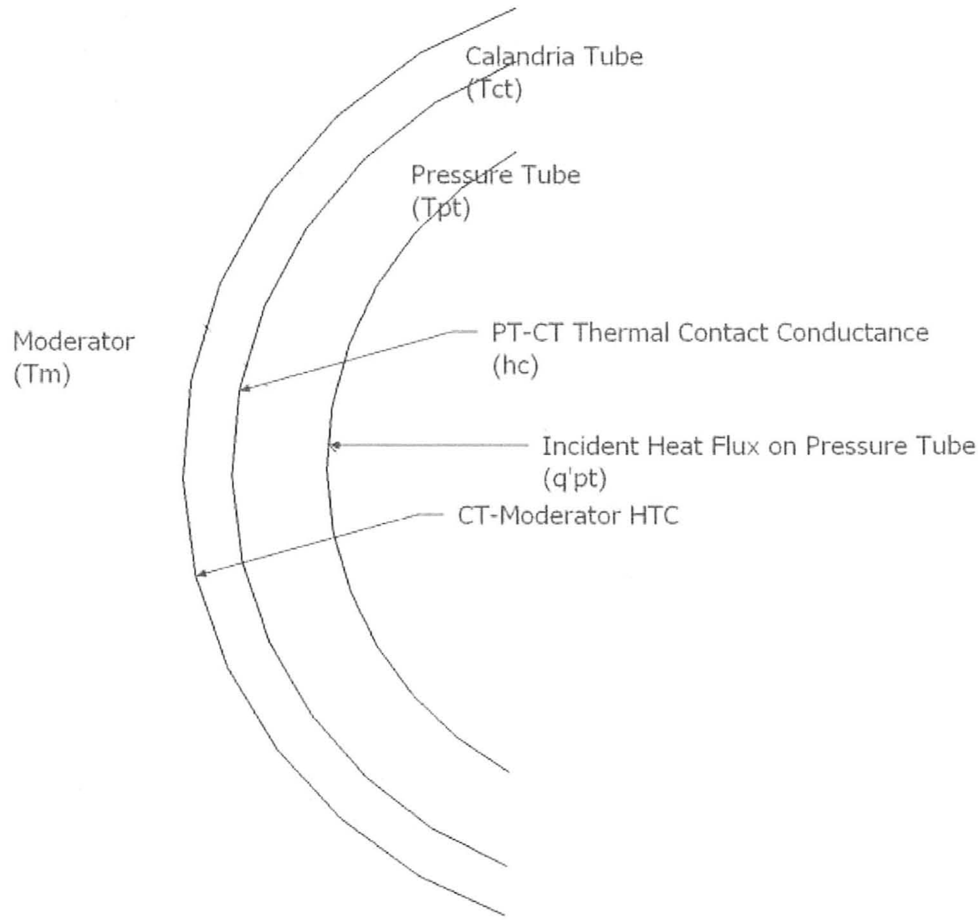

Figure 3.6: Heat transfer variables for CT in contact with PT

well as the heat flux to the moderator from the outside of the calandria tube. All of the parameters seen in Figure 3.6 are included in the following two simultaneous lumped parameter equations (Luxat, 2002);

$$m'_{pt}c_{ppt}\frac{dT_{pt}}{dt} = q'_{pt} - h'_{eff}\left(T_{pt} - T_{ct}\right) \tag{3.9}$$

$$m'_{ct}c_{pct}\frac{dT_{ct}}{dt} = h'_{eff}\left(T_{pt} - T_{ct}\right) - h'_{conv}\left(T_{ct} - T_{m}\right) \tag{3.10}$$

Where;

$$h'_{eff} = \pi D_{ct}\left(\frac{\tau_{pt}}{2k_{pt}} + \frac{1}{h} + \frac{\tau_{ct}}{2k_{ct}}\right)^{-1} \tag{3.11}$$

3.2.1 Numerical Solution for the Temperature Equations

In order to numerically solve the heat equations in the temperature module, they need to be discretized. Using a fully explicit scheme (Patankar, 1980), equations 3.9 and 3.10 become;

$$m'_{pt}c_{ppt}\frac{T^{i}_{pt} - T^{i-1}_{pt}}{\Delta t} = q'_{pt} - h'_{eff}\left(T^{i}_{pt} - T^{i}_{ct}\right) \tag{3.12}$$

$$m'_{ct}c_{pct}\frac{T^{i}_{ct} - T^{i-1}_{ct}}{\Delta t} = h'_{eff}\left(T^{i}_{pt} - T^{i}_{ct}\right) - h'_{conv}\left(T^{i}_{ct} - T_{m}\right) \tag{3.13}$$

Where the superscripts i and $i-1$ represent the present and past timesteps respectively.

Solving for PT and CT temperatures at the present time step gives;

$$T^{i}_{pt} = \frac{m'_{pt}c_{ppt}T^{i-1}_{pt} + q'_{pt}\Delta t + h'_{eff}\Delta t T^{i}_{ct}}{m'_{pt}c_{ppt} + h'_{eff}\Delta t} \tag{3.14}$$

$$T^{i}_{ct} = \frac{m'_{ct}c_{pct}T^{i-1}_{ct} + h'_{eff}\Delta t T^{i}_{pt} + h'_{conv}\Delta t T_{m}}{m'_{ct}c_{pct} + h'_{eff}\Delta t + h'_{conv}\Delta t} \tag{3.15}$$

These equations are solved simultaneously using an iterative method. The solution is determined to be converged when the difference between the new calculated value and the previous calculated value is below a certain limit. The fully explicit scheme used will generate reliable results provided that the time step is sufficiently small. A timestep size analysis can be found in the appendix.

3.3 Creep Strain Module

The creep strain module calculates PT-CT inter facial pressure from the Shewfelt creep strain equations given in Chapter two. This is accomplished by means of several assumptions;

PT radial creep is uniform in the azimuthal direction

There is no strain in the axial direction

At initial contact, inter facial pressure increases to a maximum rapidly

After initial contact, both PT and CT creep strain rates are equal

Inputs for the creep strain rate equations are the tube temperatures and hoop strain values. Therefore, to make use of the Shewfelt equations, values for hoop stress in the tubes must be known. Hoop stress can be calculated from the radius and thickness of the tube as well as the forces (pressure) acting on the tube.

$$\sigma_{pt} = \frac{(P_{pt} - P)\, r_{pt}}{\tau_{pt}} \tag{3.16}$$

$$\sigma_{ct} = \frac{(P - P_{ext})\, r_{ct}}{\tau_{ct}} \tag{3.17}$$

Where P_{pt} is the pressure internal to the PT and P_{ext} is the pressure external to the CT.

In the code, the force exerted by the fuel bundles on the PT will not be taken into account. Because ballooning deformation is cause by large internal pressures when the fuel channel is highly pressurized, the weight of the bundles is assumed to be significantly less important than the internal pressure. In the case where the PT is depressurized, the weight of the fuel bundles will be the dominant force in PT sagging.

Not every term of the Shewfelt PT creep equation (Equation 2.22) is significant for this scenario. The α-phase power law term is only significant for lower temperatures and higher stresses. With the temperatures and stresses encountered for this specific problem, the α-phase term is two to three orders of magnitude smaller than the grain boundary sliding term. Also, the integral term on the denominator is not dependent on stress and tends to unity for this specific case. Making these assumptions, the expression for PT creep strain rate is just the numerator of the grain boundary sliding term;

$$\dot{\epsilon_{pt}} = 5.7 \times 10^7 \sigma_{pt}^{1.8} exp\left(-29200/T_{pt}\right) \tag{3.18}$$

Assuming an internal pressure of 4 MPa, the hoop stress on the PT is approximately 50 MPa using Equation 3.16. For this value of PT hoop stress the plot seen in Figure 3.7 was generated to show the behaviour of Equation 3.18. At a temperature of 770 $°C$ the grain boundary creep strain rate is 4.6 $\%/s$ while the alpha creep rate is much lower at 0.00125 $\%/s$.

It should be noted that the pressure tube must undergo a total strain of approximately 16 % before it contacts the calandria tube. As the PT expands its radius is

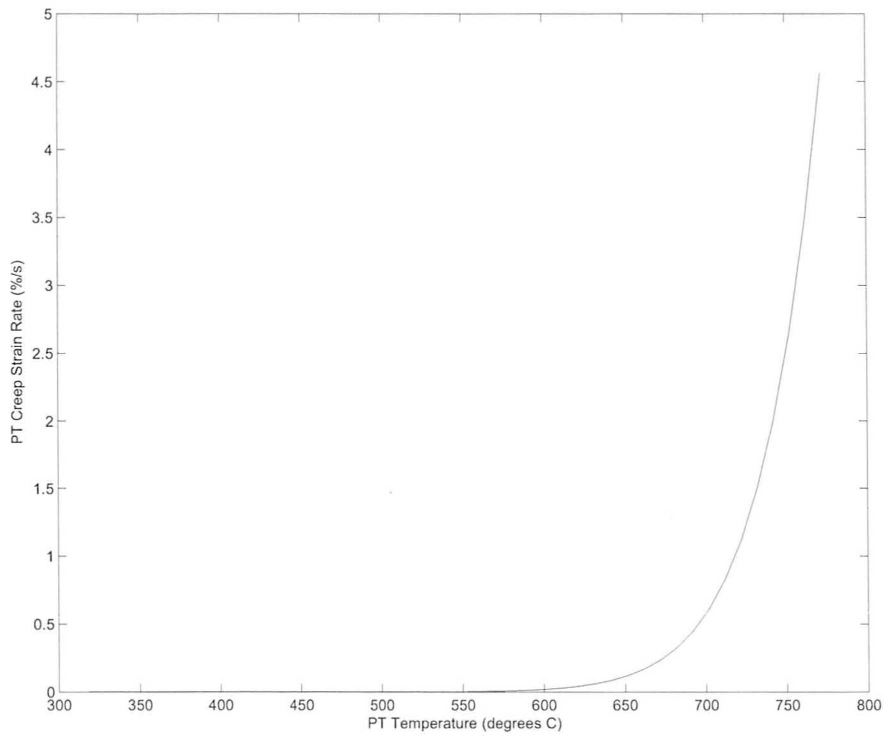

Figure 3.7: PT creep strain rate as a function of temperature with internal pressure of 4 MPa

increasing, but due to conservation of total volume of material, the thickness of the PT must decrease. This will cause PT stress to increase as can be seen from Equation 3.16 and will have an effect on the total creep strain transient of the pressure tube. Therefore we must be able to calculate PT thickness and radius as a function of hoop strain (ϵ_θ). If the tube has an outer radius, a, and an inner radius, b, then;

$$\pi\left(a^2 - b^2\right) = Const. \tag{3.19}$$

If wall thickness is $\tau = a - b$ and mid radius is $r = \frac{a+b}{2}$ then;

$$a = \frac{2r+\tau}{2}\ and,\ b = \frac{2r-\tau}{2} \tag{3.20}$$

Substituting back into Equation 3.19;

$$\left(\frac{2r+\tau}{2}\right)^2 - \left(\frac{2r-\tau}{2}\right)^2 = Const. \tag{3.21}$$

Expand and simplify to get;

$$r_t\tau_t = r_o\tau_o = Const. \tag{3.22}$$

Using the following equation for a changing radius;

$$r_t = r_o(1+\epsilon_\theta) \tag{3.23}$$

We can obtain a similar expression for thickness;

$$\tau_t = \frac{\tau_o}{1 + \epsilon_\theta} \tag{3.24}$$

Equations 3.23 and 3.24 are used in the creep strain module to calculate new values for radius and thickness as the PT experiences ballooning deformation.

Once PT-CT contact is made, the calandria tube creep strain equations from Chapter two need to be solved as well. CT stress is calculated based on Equation 3.17. Since CT temperature depends on the heat transfer from CT to the moderator, the amount of strain the calandria tube experiences can vary greatly. Figure 3.8 shows the dislocation, grain boundary and total creep strain rates for a stress of approximately 180 MPa which corresponds to a 4 MPa contact pressure. For the temperature range shown both modes of deformation are significant, but for higher temperatures the grain boundary term becomes negligible.

The center of this mechanistic model relies on solving this simultaneous system of creep strain equations. In order to find a solution, it is required to develop some way of relating the two sets of creep strain relations for PT and CT. During the initial contact and post-contact phases, the two tubes move together. Therefore we can impose the condition;

$$\dot{\epsilon_{pt}} = \dot{\epsilon_{ct}} \tag{3.25}$$

By applying this boundary condition, we can solve for the stress in each tube and consequently the interfacial pressure in between the tubes. The structure of the creep strain module is designed to use iterative methods to solve five simultaneous equations. A flow chart is shown in Figure 3.9. In the pre-contact phase, only the

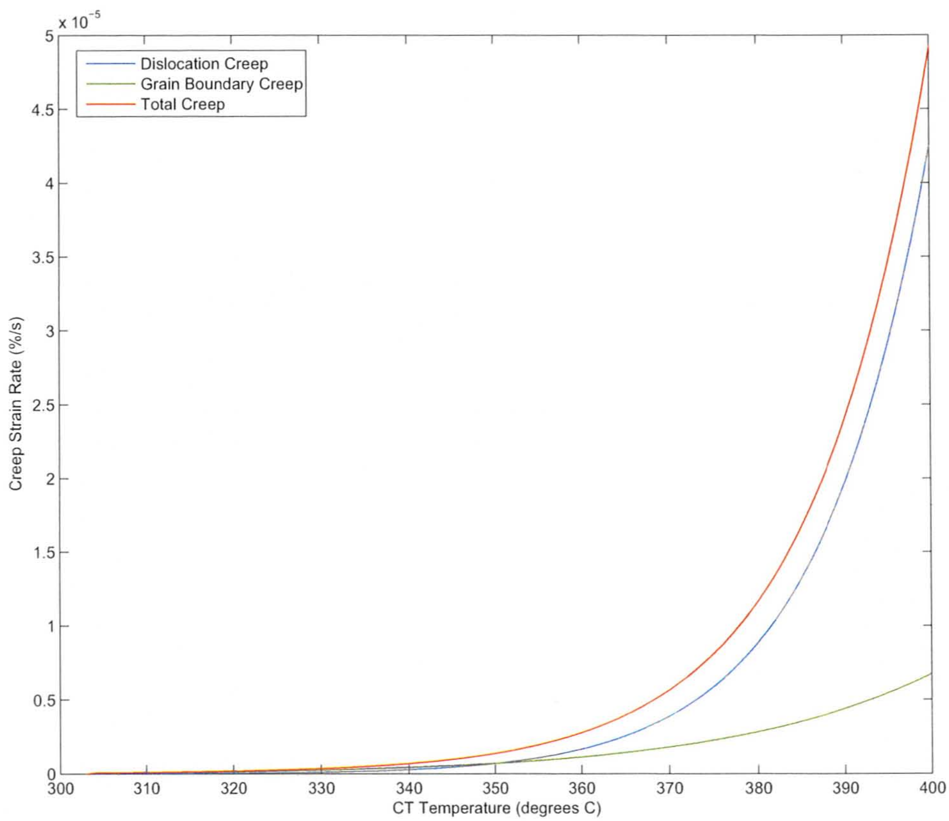

Figure 3.8: CT dislocation, grain boundary and total creep strain rates as a function of temperature with inter facial pressure of 4 MPa

pressure tube creep strain equation is used to calculate PT ballooning under its own internal pressure. Once contact occurs, a contact pressure value, P, as well as a σ_i value is guessed. Dislocation creep strain rate, $\dot{\epsilon_d}$, is iteratively solved for using the two dependent equations 2.24 and 2.25. The second iterative loop uses the condition imposed in Equation 3.25 and uses it to calculate a new value of contact pressure from Equation 2.22. Once the difference between the new calculated contact pressure and the previous value of contact pressure is below the convergence criteria, δ, the contact pressure solution is obtained.

It should be noted that the condition imposed in Equation 3.25 is a direct result of the third and fourth assumptions made in the creep strain module. If these two assumptions are relaxed, in particular the fourth assumption, just following initial contact a thin layer of the CT inner surface would heat up to a much higher temperature than the rest of the tube, which could be approximated by utilizing a one dimensional radial conduction model in the temperature module. Since the majority of the CT is at a lower temperature it will not expand immediately. Even further, the surface asperities on the hot inside region of the CT will deform. These effects are expected to lead to a large but very brief spike in TCC immediately following initial contact. The time scale of this transient feature is much smaller than the time step used in the computer model therefore the initial contact assumptions are enforced.

Immediately after PT-CT contact is made, the code solves both Shewfelt creep strain rate equations simultaneously. This results in contact pressure increasing to its maximum value instantaneously after PT-CT initial contact. An analysis was completed to calculate an estimate for contact pressure ramp up time and the resulting plot can be seen in Figure 3.10. Pressure values were normalized for the plot and

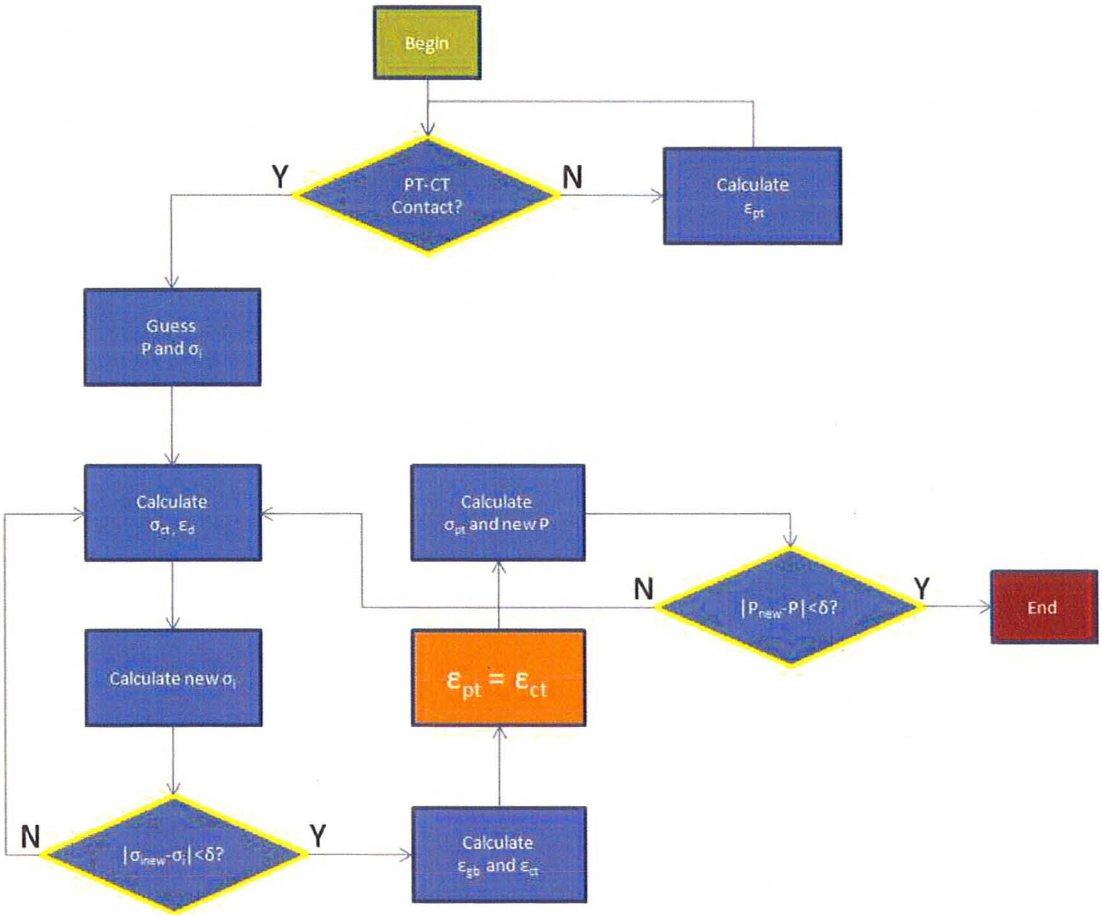

Figure 3.9: Flow chart illustrating structure of the creep strain module

the PT internal pressure was 4 MPa for the calculation. Just prior to contact, the creep strain rate of the pressure tube is very high (approximately $5\,\%/s$). Assuming elastic deformation of the calandria tube for the time immediately following PT-CT contact, it was determined that contact pressure will reach its maximum value within a common value of time step used in the code ($0.1\,s$). By comparing this time to the length of the entire event, an instantaneous pressure ramp up can be justified as a valid assumption.

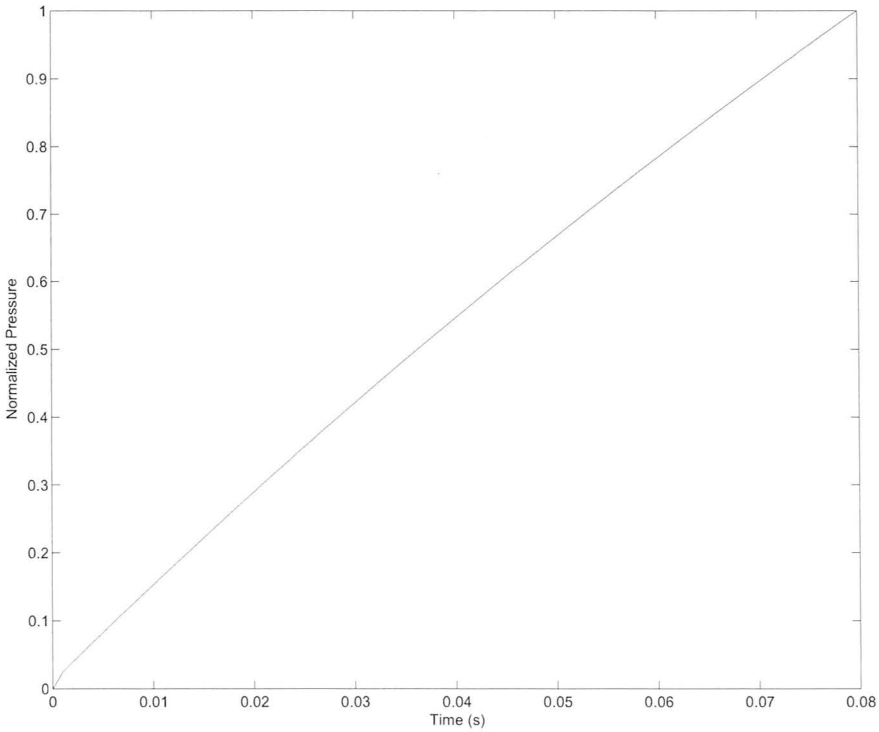

Figure 3.10: Normalized contact pressure vs time for estimated contact pressure ramp-up

3.4 Code Assembly

The three modules are assembled as shown in the flow chart Figure 3.11. The conductance module comes first and only calculates TCC if PT-CT contact has occurred. The temperature module comes second and iteratively solves both PT and CT heat equations. The creep strain module comes last and uses the temperatures determined in the temperature module to solve the creep strain equations if PT-CT contact has occurred. Otherwise it just determines PT ballooning. Figure 3.9 shows the creep strain module in more detail. When a new value for contact pressure is solved for, the time step is incremented and the loop is repeated for the next time step. This method allows the prediction of TCC values for the entire PT-CT contact transient. At the beginning is the input file which holds all of the initial conditions, and paramters which may be changed by the user. These include surface characteristic values, PT internal pressure, PT incident heat flux, CT-moderator heat transfer characteristics, initial temperatures, length of transient, and size of time step.

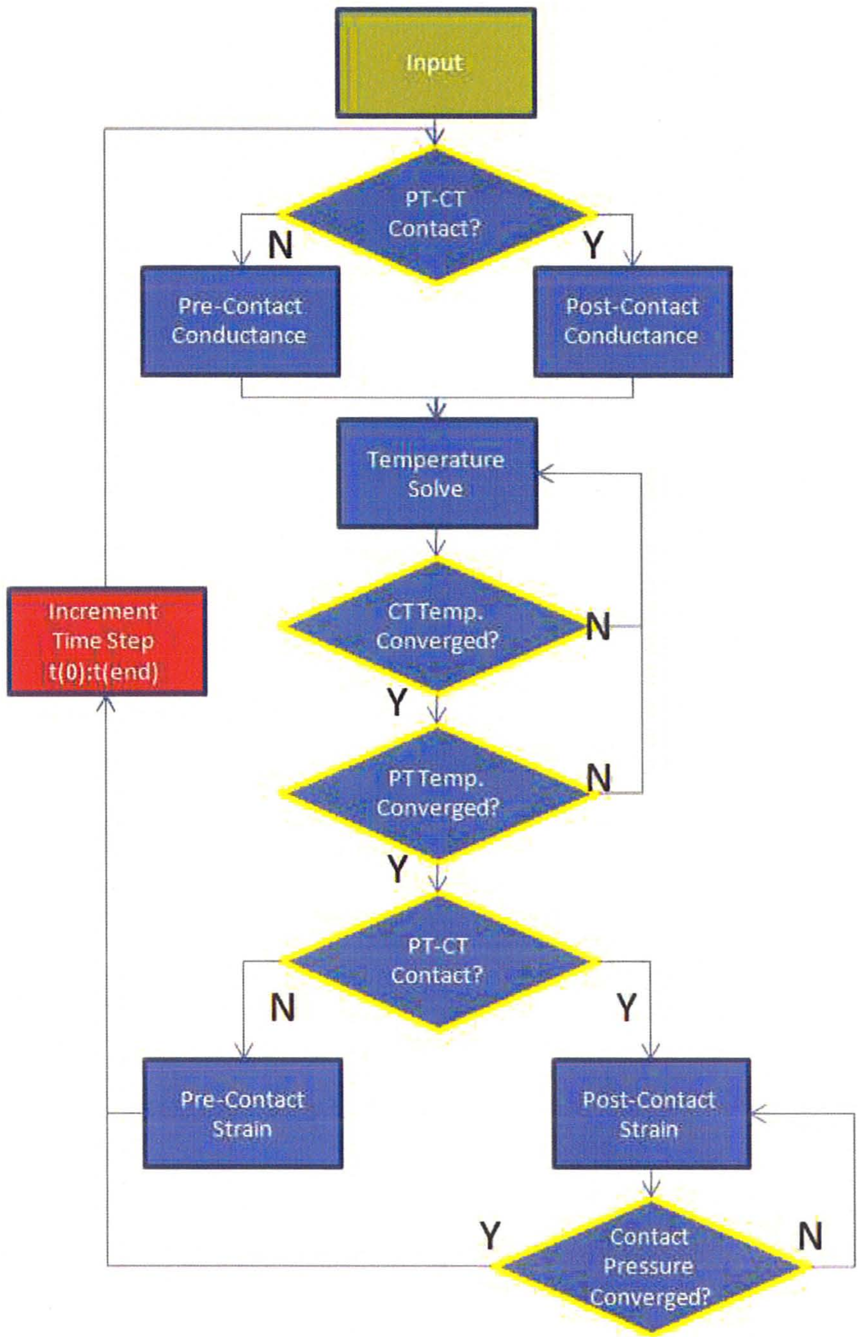

Figure 3.11: Flow chart illustrating overall code structure

Chapter 4

Results and Analysis

In this chapter some general results and characteristics of code output is presented. Various aspects of the model output is interpreted and explained including the behaviour of; TCC, temperature, and creep strain transients. A sensitivity analysis is done to determine the effect of various parameters on TCC transient results. Contact conductance transient data is extracted using results from several graphite heater contact boiling experiments. Results from the mechanistic model is then compared to experimental data.

4.1 General Code Results and Behaviour

Two sets of general results from the mechanistic model using different boundary conditions for CT-moderator heat transfer coefficient are shown in Figures 4.1 and 4.2. The first case illustrates temperatures and TCC transient values for a high value of h_{conv} representing no film boiling on the CT outer surface. The second case shows results for a low value of h_{conv} representing the heat transfer that would occur if film boiling did occur on the CT outer surface.

Figure 4.1 represents a case where no film boiling is observed. This is established by fixing the pool boiling convective heat transfer coefficient between the calandria tube and the moderator at $50\,kW/m^2/^\circ C$. This falls within the expected range for natural convection heat transfer (Luxat, 2002). The PT incident heat flux boundary condition was $25\,kW/m$. During the heatup phase, the pressure tube heats up approximately linearly. When contact is made, there is a sharp decrease in temperature as heat is transferred from PT to moderator via the calandria tube. CT temperature does not rise significantly because no nucleate boiling or dryout occurs on the CT surface (high h_{conv}, this results in no CT creep strain deformation. PT-CT contact conductance is high at initial contact, (approximately $11\,kW/m^2/^\circ C$) when contact pressure is at its highest. This value quickly decreases as the pressure tube temperature decreases. The steady state value settles to approximately $5\,kW/m^2/^\circ C$.

When CT-moderator heat transfer is limited by a small heat transfer coefficient, as would be the case in calandria tube dryout, CT temperature at contact rises to a higher level. Figure 4.2 shows the results in which the convective heat transfer coefficient was fixed at $1\,kW/m^2/^\circ C$. Incident heat load on the pressure tube remains at $25\,kW/m$. The peak and steady state values of contact conductance remain the same as the case with no film boiling in figure 4.1, but the time to reach steady values in the post-contact phase is considerably longer. Since the CT experiences higher temperatures, it undergoes a small amount of creep at initial contact. The calandria tube creep results in an initial rapid drop in contact pressure and therefore a decrease in conductance followed by a slight recovery as the pressure tube expands

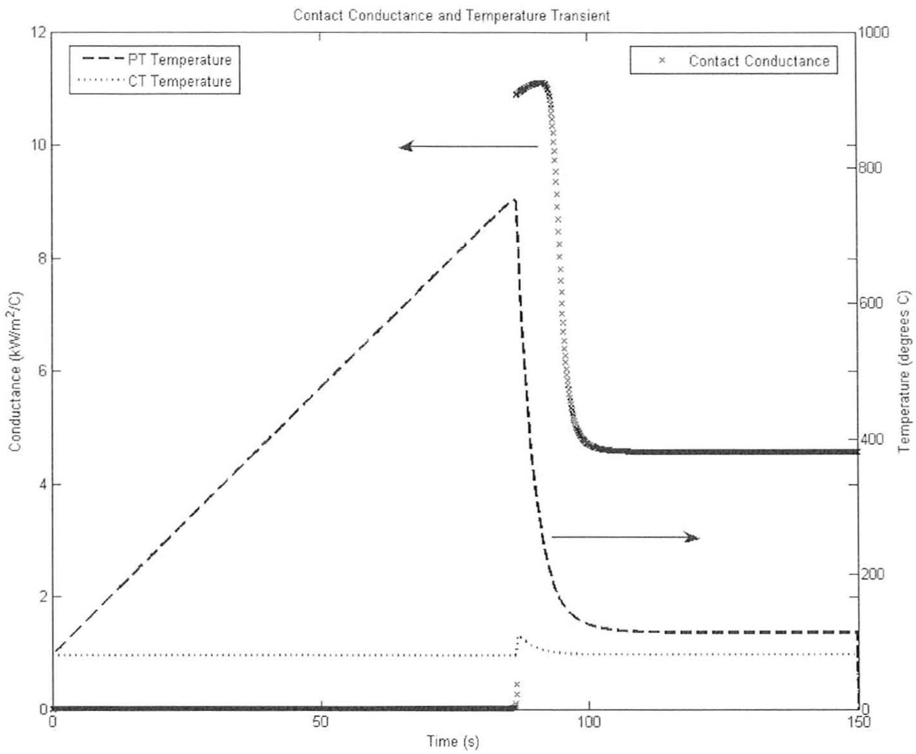

Figure 4.1: TCC and temperature transients for high CT-moderator heat flux

further.

Figures 4.3 and 4.4 are plots of the transient stress and strain in the two tubes, respectively. These plots are for the case where the h_{conv} boundary condition has a small value. In the stress plot, PT stress is constant during the majority of the heat up phase. This is because the internal pressure of the PT remains constant in the model simulation. As the PT heats up it starts to creep. A positive creep in the azimuthal direction results in negative radial creep strain and thinning of the tube wall which explains the increase in PT strain just prior to PT-CT contact (Equation

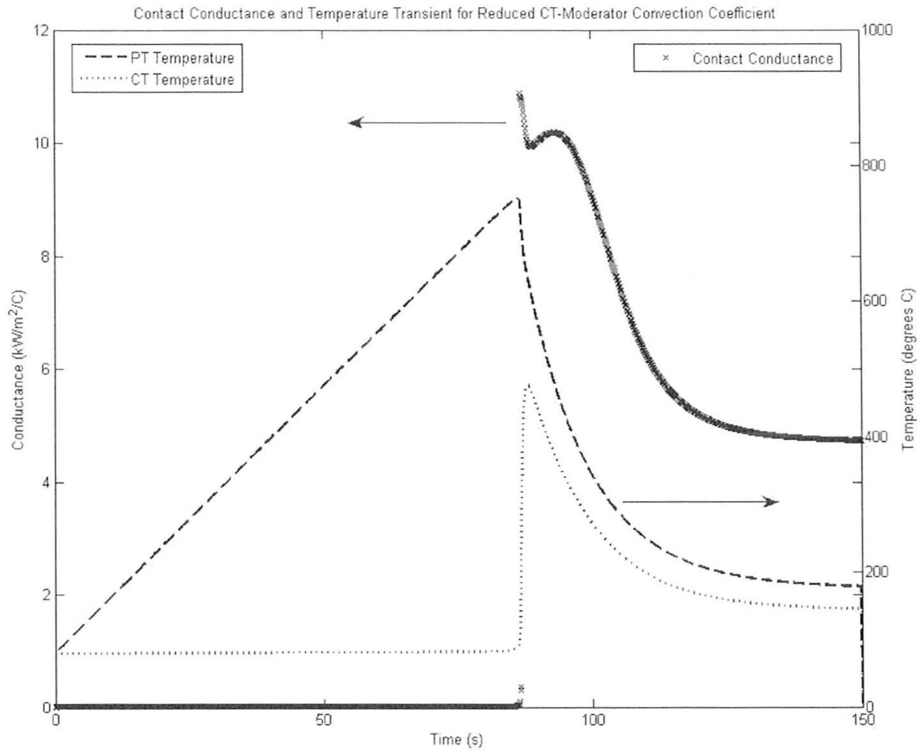

Figure 4.2: TCC and temperature transients for low CT-moderator heat flux

3.16). Calandria tube stress is zero until PT-CT contact is made. Immediately after contact CT stress jumps to a high value because of high initial contact pressure. CT stress then decreases with contact pressure. A mirroring effect can be seen in PT stress after initial contact as the contact pressure between PT and CT serves to decrease stress in the pressure tube.

The creep strain rate of the PT increases fairly rapidly once a certain threshold temperature is reached as can be seen in Figure 3.7 and is consistent with the transient results shown in Figure 4.4. High PT creep strain rate means rapid ballooning of

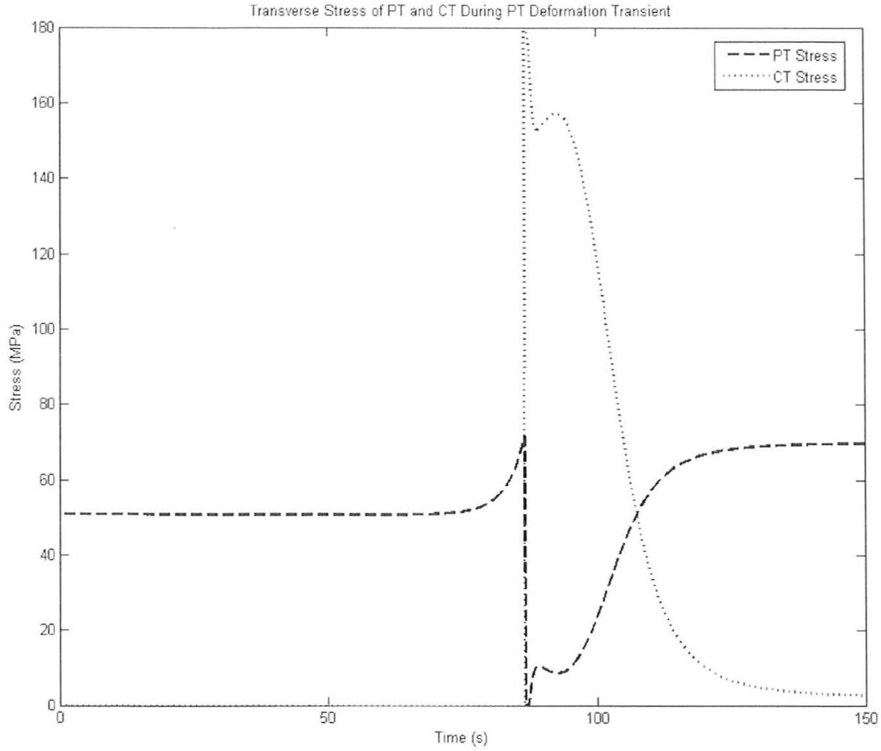

Figure 4.3: Calculated stress transient for CT and PT

the pressure tube into contact with the calandria tube. Shortly after contact, CT temperature increases. High temperature and stress in the calandria tube leads to a small amount of CT creep. Note that the transient stress and strain plots represent the case where CT-moderator heat transfer is limited. For high CT-moderator heat transfer, CT creep is negligibly small due to CT temperature remaining low.

In general, the shape of the TCC transient is very similar to the inter facial pressure transient. This is because contact pressure is one of the key parameters influencing contact conductance. The main solid conductance equation (Equation

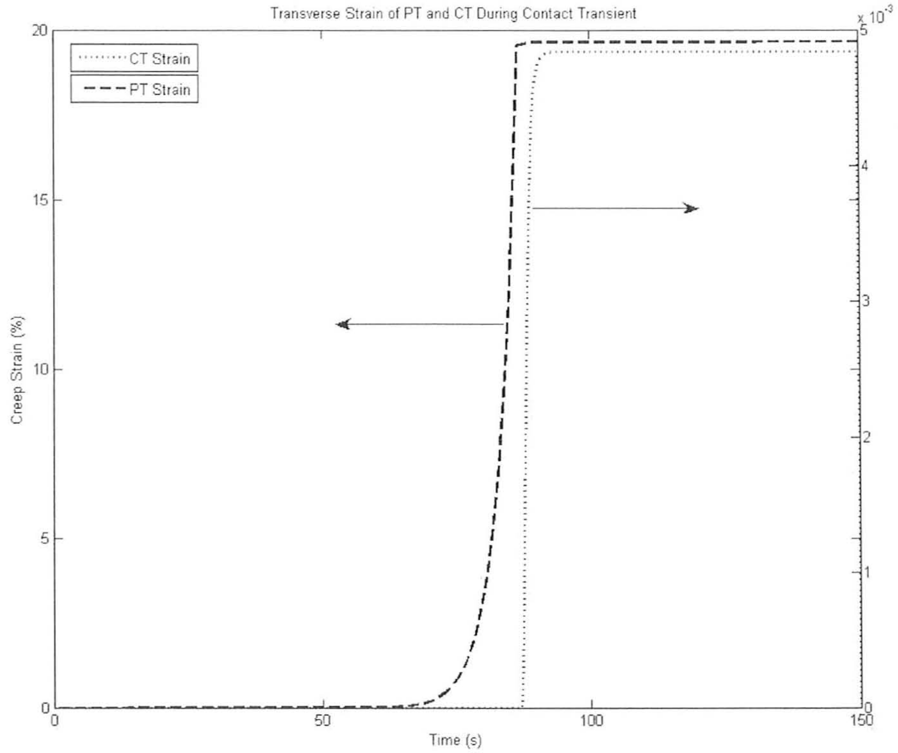

Figure 4.4: Calculated creep strain transient for CT and PT

2.15) shows an almost linear relationship between contact pressure and solid contact heat transfer coefficient. Contact pressure is also the most important parameter which changes dramatically over the course of the PT-CT contact event. A plot of contact pressure with respect to time would look the same as a TCC plot but with a maximum contact pressure peak at approximately the value PT internal pressure.

4.2 Sensitivity Analysis of Key Parameters

There are many key parameters which influence the PT-CT thermal contact conductance transient. Understanding which variables have a significant effect as well as their overall effect on the system is important. Some of the key parameters were briefly discussed in section 3.1 and includes surface characteristics such as roughness as well as the ratio of contact pressure to surface hardness. The goal of this thesis is to model a TCC transient, therefore in this section, a sensitivity analysis will be performed for the parameters of key importance to the Yovanovich model.

Sensitivity analysis is used to propagate uncertainties through complex systems, where manually doing so could be excessively cumbersome. By using these techniques a large amount of data can be recovered without performing large amounts of code simulations. An example equation used in dynamic sensitivity analysis is:

$$X = X_0 + \frac{\partial X}{\partial Y} \Delta Y \tag{4.1}$$

Where the X parameter is a function of some parameter, Y, and X_0 is the value of X without any perturbation. If Y is changed by some amount, δY, then X is an approximation of the resulting output.

Dynamic sensitivity analysis is a method which allows the study of key parameters and their effect over an event transient. Dynamic sensitivity functions are analytical partial derivatives of the equations used in modeling the system. They are evaluated using transient reference trajectories for the other variables which have been calculated from simulations using the mechanistic model (Luxat, 2008). Dynamic sensitivity functions are derived for surface roughness and the ratio of contact pressure to surface hardness as seen below.

$$W1 = \frac{\partial h_c}{\partial \sigma} \quad W2 = \frac{\partial h_g}{\partial \sigma} = \frac{\partial h_g}{\partial Y}\frac{\partial Y}{\partial \sigma} \tag{4.2}$$

$$W3 = \frac{\partial h_c}{\partial P/H} \quad W4 = \frac{\partial h_g}{\partial P/H} = \frac{\partial h_g}{\partial Y}\frac{\partial Y}{\partial P/H} \tag{4.3}$$

The effect of each variable can easily be seen by plotting the sensitivity functions for the variable in question. Figure 4.5 shows the sensitivity of solid and gas gap conductance to PT-CT mean surface roughness. Initial contact occurs at 85 s and it can be seen that roughness holds the greatest importance to solid contact conductance at the instant of contact and just afterwards. In the post-contact phase, $W1$ becomes less important because a lowering of contact pressure causes the gas gap conductance to be the more dominant effect. The effect of roughness on gas gap conductivity is somewhat more significant in the post-contact phase. This is because mean surface roughness values play a different role in the behaviour of gas gap conductivity. Instead of being used to give an approximation of the amount of solid contact area, roughness is used to give an approximation for mean plane separation so that conduction through the gas gap can be estimated. The maximum magnitude of $W2$ is seen approximately 6 s after initial contact. This is due to the effect of the mean free path and accommodation parameters in the gas gap conductivity equations.

Perhaps the most important term in all of the TCC correlations is the ratio of inter facial contact pressure to surface hardness. The sensitivity functions $W3$ and $W4$ represent the sensitivity h_c and h_g to this ratio. In Figure 4.6 they are evaluated about reference response trajectories for contact pressure as well as the correction term $\alpha_a\beta\Lambda$ in the case of $W4$.

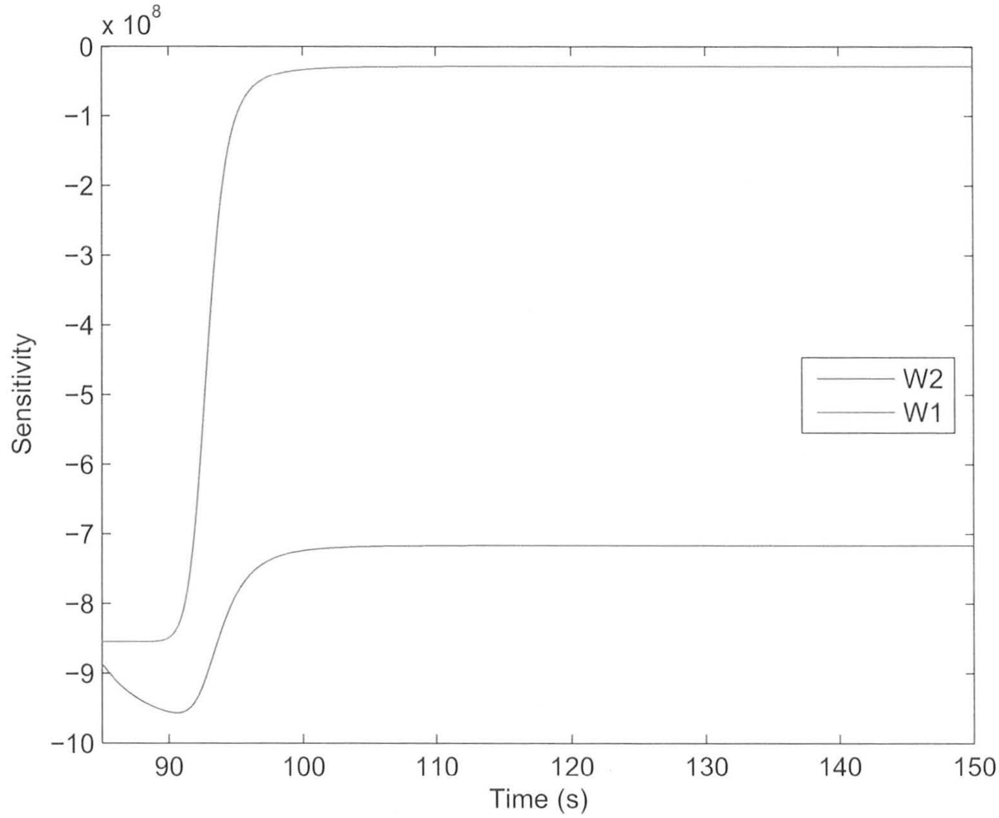

Figure 4.5: Dynamic sensitivity of solid contact and gas gap conductance, Functions W1 and W2, to mean surface roughness

The sensitivity function $W4$ is low in the initial contact phase and increases as contact pressure decreases in the post-contact phase. The solid contact sensitivity function exhibits similar behaviour but varies by less overall during the transient. The behaviour of these two terms leads to the inference that the P/H ratio is more important in the post-contact phase especially for gas gap conductance. It is known that gas gap conductance is the dominant mode of heat transfer for the lower contact pressures which are present in the post-contact phase. Therefore, the long term heat transfer characteristics of the system after contact are heavily dependent on contact

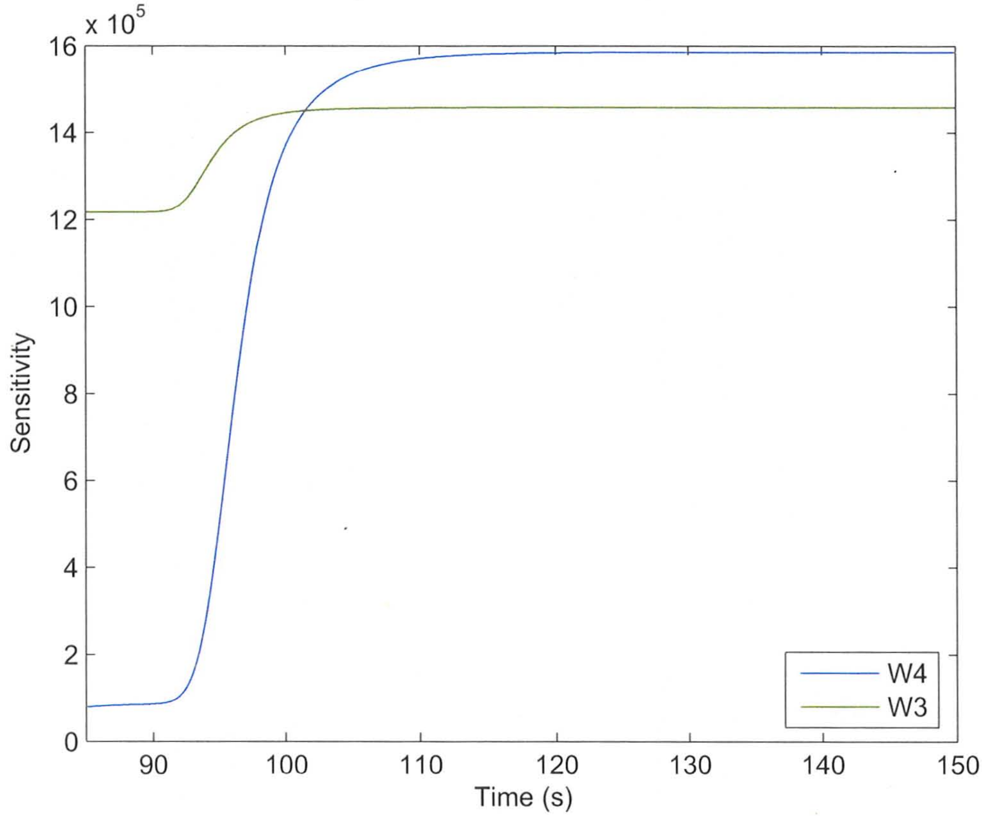

Figure 4.6: Dynamic sensitivity of solid contact and gas gap conductance, Functions W3 and W4, to the ratio of contact pressure and surface hardness

pressure.

There are many variables which affect the post-contact PT-CT interstitial pressure but for the most part it is determined by the strain of the two tubes in this phase . The strain behaviour is in turn influenced by the boundary conditions of PT incident heat flux and CT-moderator heat flux. For example, if the incident heat flux on the pressure tube from the fuel is high, and CT-moderator heat flux is also high, harder contact between PT and CT will result. This is because the calandria tube will not significantly deform and since the creep strain rates of the two tubes are equal, contact pressure must be large. If for the high PT incident heat flux condition, CT film boiling occurs contact pressure between the two tubes will be lower due to higher CT creep. Under low PT incident heat flux conditions, contact pressure will tend to stay low in the post-contact phase and also CT-moderator heat transfer is less important.

4.2.1 Sensitivity of TCC to CT-Moderator HTC

The CT-moderator heat transfer coefficient plays a major role as a boundary condition in the mechanistic model. The effect of CT-moderator heat transfer determines how much the CT will deform and is therefore important to the value of PT-CT contact pressure and ultimately, fuel channel integrity. Studying the sensitivity of thermal contact conductance to CT-moderator HTC is a complicated issue because the variables in question span all three modules of the developed mechanistic model. The dynamic sensitivity methodology will be used to propagate this value through the three modules.

In order to propagate uncertainty in the convective heat transfer between calandria tube and moderator, sensitivity parameters must be developed spanning all three modules of the code. The sensitivity parameters are:

$$W5 = \frac{\partial T_{pt}}{\partial h'_{conv}} \quad W6 = \frac{\partial P}{\partial T_{pt}} \quad W7 = \frac{\partial h}{\partial P} = \left[\frac{\partial h_g}{\partial Y}\frac{\partial Y}{\partial P} + \frac{\partial h_c}{\partial P}\right] \tag{4.4}$$

The three sensitivity parameters are combined to give:

$$\frac{\partial h}{\partial h'_{conv}} = W5 \cdot W6 \cdot W7 \tag{4.5}$$

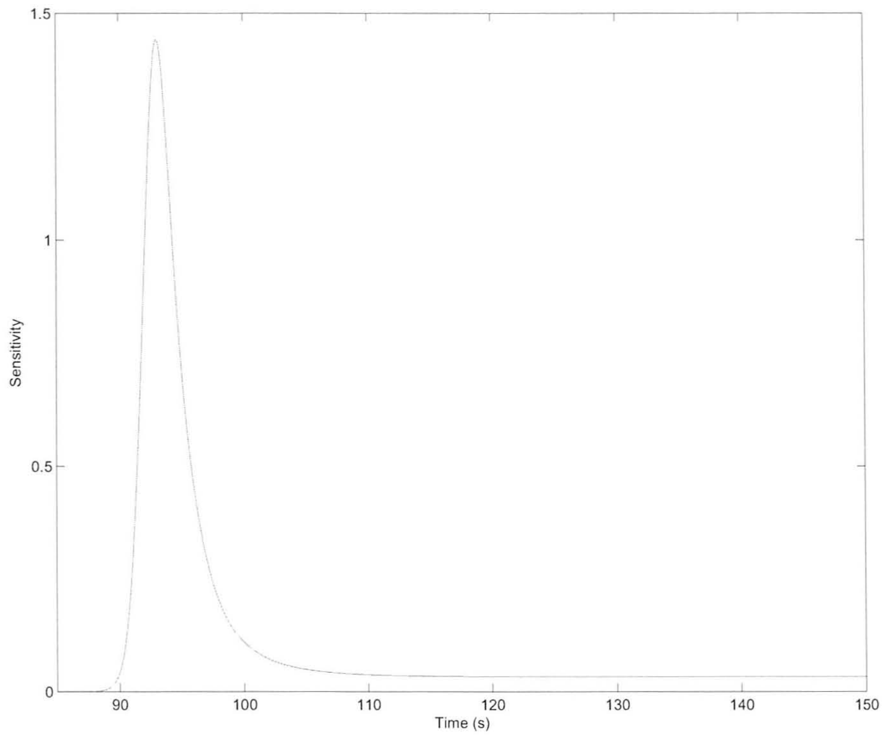

Figure 4.7: Dynamic sensitivity of PT-CT thermal contact conductance to CT-moderator heat transfer coefficient

By plotting the final sensitivity parameter (Equation 4.5) about the reference trajectories for all the variables present in each module, Figure 4.7 is created. As with the previous sensitivity plots PT-CT contact occurs at approximately $85\,s$. The plot shows a somewhat small dependency of TCC on CT-moderator heat transfer with the exception of a large spike from $90\,s$ to $100\,s$. This peak comes a few seconds after the maximum PT-CT heat flux values which are at initial contact. CT-moderator heat transfer has an large effect in this specific time range because the calandria tube has just received a significant amount of thermal energy. In this phase, CT deformation will depend on how much of this thermal energy it is able to transfer to the moderator. As discussed on page 60 the thermal contact conductance transient is greatly affected by the amount of CT deformation in the initial contact phase.

Since it is known that the PT-CT TCC transient is dependent on CT-moderator heat transfer, a way to model this portion of the system must be used. The correlation for pool boiling heat transfer developed by Rohsenow (Carey, 2008) can give an approximation for CT-moderator heat transfer:

$$\frac{q''}{\mu_l h_{lv}}\sqrt{\frac{\sigma}{g\left(\rho_l-\rho_v\right)}}=\left(\frac{1}{C_{sf}}\right)^{1/r}Pr_l^{-s/r}\left[\frac{c_{pl}\left[T_w-T_{sat}(P_l)\right]}{h_{lv}}\right]^{1/r} \tag{4.6}$$

Where, $C_{sf}=0.013$, $s=1.0$ and $r=0.33$ for the water-zircaloy interface in question.

The Rohsenow equation relates heat flux to the temperature difference between liquid and solid surface. This means that if either heat flux or temperature difference is known, the pool boiling convective heat transfer coefficient can be calculated as;

$$h'_{conv}=\frac{q''_{ct-mod}}{T_{ct}-T_{sat}(P_{mod})} \tag{4.7}$$

Utilizing this method, reasonable values for CT-moderator HTC can be obtained and implemented in the model.

4.3 The Effect of Surface Roughness and Asperity Slope

In the Yovanovich TCC equations there are terms for mean surface roughness and mean surface asperity slope. The surface roughness term is present in both the solid contact and gas gap equations. The asperity slope term is only present in the solid contact equation. If the m/σ ratio changes it can vary the relative magnitudes of the solid and gas gap terms. An analysis was done for several TCC transients using different m/σ ratios while keeping the peak contact conductance values the same. For a higher value of m/σ, conduction through the gas gap is lower relative the the solid contact conductance. This results in a lower value of TCC in the post-contact phase because it is in this region that gas gap conductance tends to be the dominant mode of TCC. The resulting plot from this analysis can be seen in figure 4.8. PT internal pressure was 3.6 MPa. A new parameter used in evaluating TCC transients can be defined as the ratio of peak TCC values to post-contact equilibrium values of TCC. This will be referred to as the P/L ratio. Table 4.1 shows the values of P/L ratio with varying m/σ ratio in this analysis. This information can prove to be valuable for

Table 4.1: m/σ vs. P/L ratios

$m/\sigma(mm^{-1})$	P/L
4.753	1.399
14.29	1.533
25.32	1.720
33.86	1.904
40.82	2.083
46.73	2.259
51.72	2.431
55.73	2.600

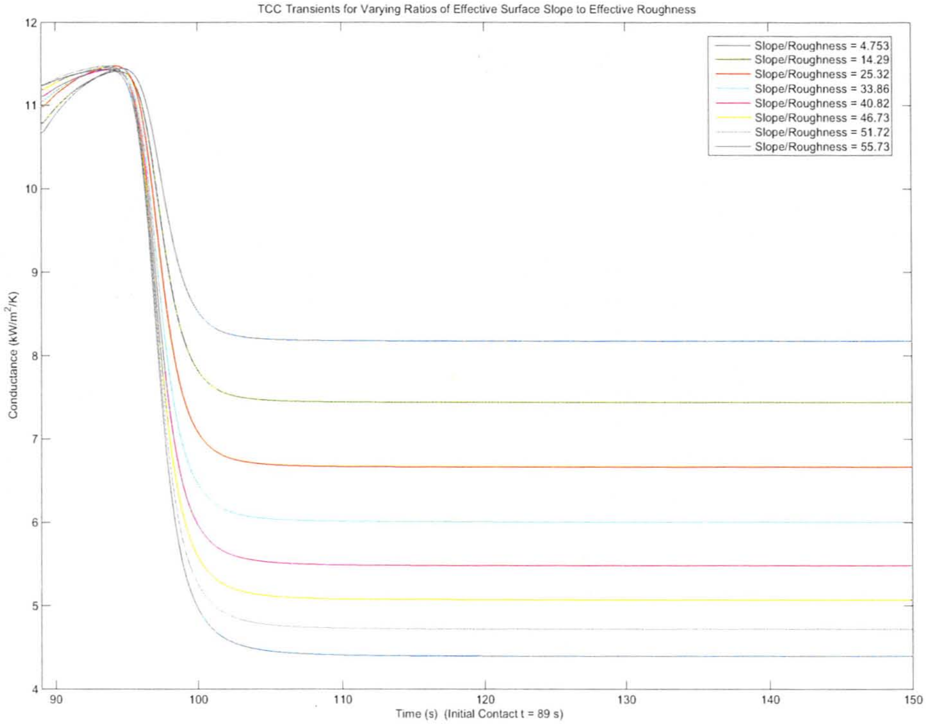

Figure 4.8: TCC transient for varying surface asperity slope to surface roughness ratio

calibration of the computer model where surface characteristic values are not known. This is done by selecting a value of m/σ which gives a good P/L ratio for one set of experimental data. The same values can then be used for validation with another, independent data set.

4.4 Contact Pressure Results

In Luxat (2002) an expression for inter facial pressure between PT and CT is given (equation 2.27). This expression is a function of PT internal pressure, CT external pressure and a pressure redistribution factor. In figure 4.9 the results from the equation are plotted against results obtained from a model simulation for a contact boiling test. The solid black line represents perfect agreement and the dotted black lines represent an error of $\pm 5\,\%$. The results show good agreement between predicted

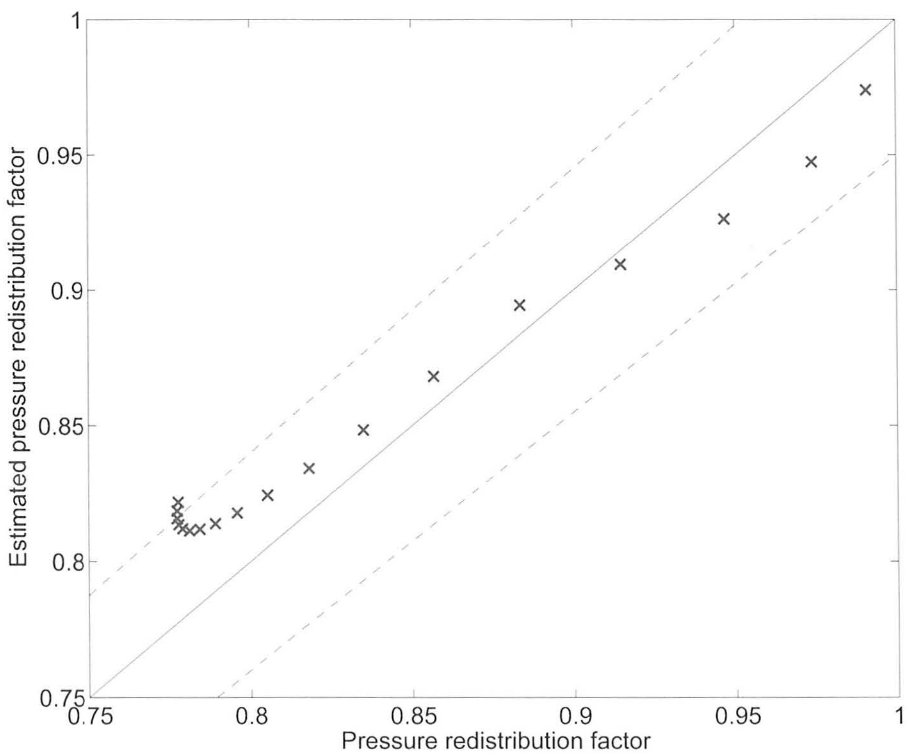

Figure 4.9: Model prediction for pressure redistribution factor as a function of redistribution factor from Luxat (2002)

values and values given by the equation, especially in the region of high pressure redistribution factor. For this example there is a slight over prediction of approximately 5 % as the redistribution factor reaches lower values.

4.5 Treatment of Experimental Data

A comparison of experimental data to the mechanistic model presented in this report should be conducted for validation purposes. Many contact boiling experiments have been performed by various organizations with the intent of studying fuel channel behaviour for a PT-CT contact event. Typically these experiments involve a section of a CANDU fuel channel submersed in a pool of water. A graphite heater is used to provide the incident heat flux on the inside of the pressure tube. Many sets of thermocouples are arranged in rings at several axial positions along both the pressure tube and the calandria tube. PT thermocouples are welded into place through holes drilled in the pressure tube. Their location is at the middle of the PT thickness. CT thermocouples are spot welded to the outside of the calandria tube. Various values of heater power, moderator subcooling as well as PT internal pressure are used in different tests.

One challenge faced when studying contact boiling experiments is the extraction of PT-CT TCC values. Since only PT and CT temperatures can be recorded, a valid method of determining the contact conductance transient must be developed. One type of approach used in the past was to estimate PT-CT contact heat flux by using data for heater power in conjunction with heat removal from the water tank (H.Z. Fan, 2002). This approach just gives an average value of TCC and is not sufficient for studying the TCC transient at and following the instant of contact. A

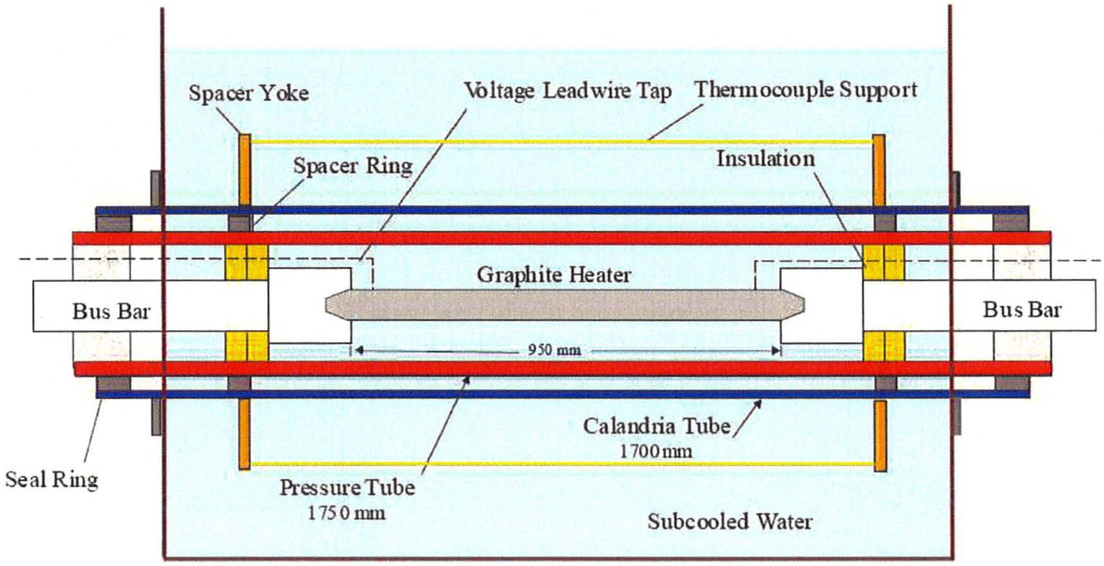

Figure 4.10: Example cross section of contact boiling experiment apparatus (Neal and Fraser, 2003a)

possible method of TCC extraction involves using the general heat transfer equations for PT and CT. Then, the equations can be solved for TCC using the transient temperatures.

Equations 3.9 and 3.10 are rearranged and solved for h'_{eff} to give:

$$h'_{eff} = \frac{m'_{ct}c_{pct}\frac{dT_{ct}}{dt} - m'_{pt}c_{ppt}\frac{dT_{pt}}{dt} + q'_{pt} + h'_{conv}\left(T_{ct} - T_m\right)}{T_{pt} - T_{ct}} \tag{4.8}$$

Since the PT thermocouples are in the middle of the tube thickness and CT thermocouples are positioned on the outside of the tube, the effective contact conductance between the two tubes is:

$$h'_{eff} = \pi D_{ct}\left(\frac{\tau_{pt}}{2k_{pt}} + \frac{1}{h} + \frac{\tau_{ct}}{k_{ct}}\right)^{-1} \tag{4.9}$$

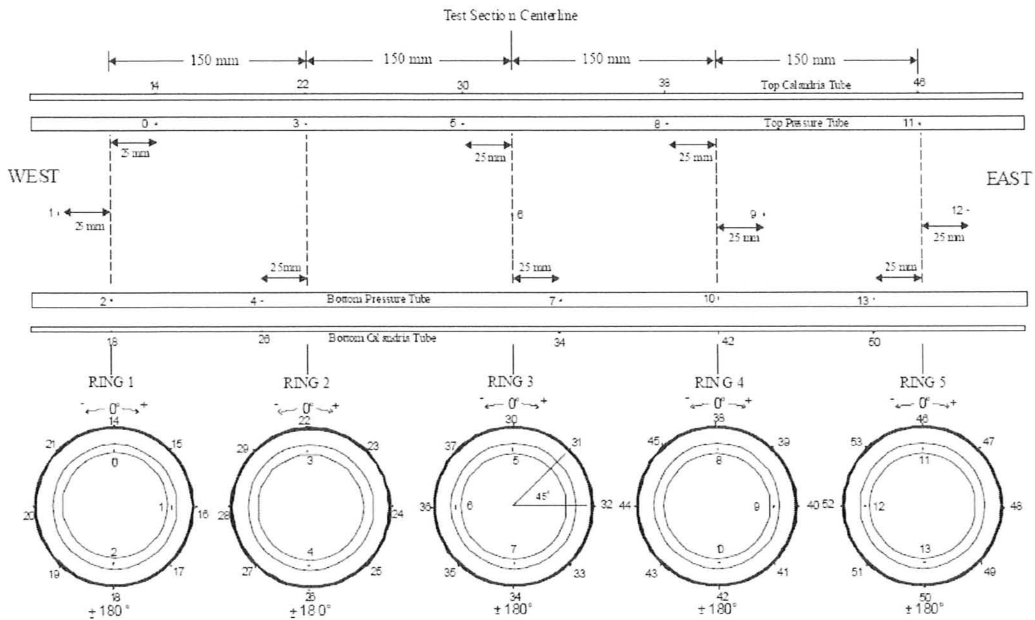

Figure 4.11: Depiction of thermocouple locations for contact boiling experiment (Neal and Fraser, 2003a)

Where h'_{conv} is obtained for each experiment using the Rohsenow correlation shown in Equation 4.6.

4.5.1 PT Incident Heat Flux Boundary Condition

Incident heat flux on the inside of the pressure tube is one of the boundary conditions used when modeling PT-CT contact. Experiments specify the linear heater power used for each test but this number is not equivalent to the heat given directly to the pressure tube. In order to determine the proper PT incident heat flux boundary condition, the PT heatup rate from the pre-contact phase is used in conjunction with the mass and specific heat of the pressure tube. PT heatup rates are measured and specified for all contact boiling tests. The following equation illustrates the relationship and can be derived from equation 3.9 by setting the h'_{eff} to zero which is a good approximation for the pre-contact phase.

$$q'_{pt} = m'_{pt} c_{ppt} \frac{dT_{pt}}{dt} \tag{4.10}$$

4.6 Comparison to Contact Boiling Tests

In this section, a comparison between the developed model and data from two graphite heater contact boiling experiments are made. The first set of contact heat transfer coefficient data was extracted from temperature data using the method outlined in section 4.5. The temperature data was recorded during the test by thermocouples mounted on PT and CT. The second set of data was taken from a report by H.Z. Fan (2004). CHTC was estimated for several sets of thermocouples. Test conditions are given in table 4.5. Dryout maps for the CT outer surface are shown for each test in figures C.2 and C.3. The shaded areas of each map represent areas of oxide discolouration which is indicative of dryout.

Table 4.2: Experimental conditions for two contact boiling tests

Test Name	PT Pressure	PT Heatup Rate	Subcooling	Percent CT Dryout
SUBC5	3.6 MPa	25 $°C$	36 $°C$	6 %
Q6	4.4 MPa	24.6 $°C$	22.7 $°C$	27 %

4.6.1 Comparison to Extracted Data

Experiment SUBC5 features high moderator subcooling and high PT incident heat flux conditions. This test was classified as "immediate quench" because film boiling on the CT surface was not sustained for more than 5 seconds and there was no noticeable deformation of the calandria tube. Three sets of CHTC transient data were extracted from three thermocouple pairs in one ring of the test apparatus. Thermocouple pairs were located on the top (TC8-TC38), bottom (TC10-TC42), and side (TC9-TC40) of the test section. Table 4.3 shows experimental temperatures and predicted temperatures for PT and CT along with calculated boundary condition values used for CHTC extraction and code simulation.

The large discrepancy between predicted and experimental CT maximum surface temperatures can be attributed to local dryout in some regions (approx. 6% of CT surface). No dryout condition was imposed on the CT outer surface in the SUBC5 analysis, therefore the CT outer temperature remained low.

Table 4.3: Experimental data and model predictions for SUBC5

	q'_{pt}	h_{conv}	PT Contact Temp	Max CT Temp
Experimental Data			885-903 $°C$	351 $°C$
Model Predictions	80.2 kW/m	26 $kW/m^2 \cdot °C$	797 $°C$	127 $°C$

Figure 4.12 shows the three CHTC data sets along with the model predictions for the test. The time scale is set so that initial contact occurs at time zero. It can be seen that the top of the test section experiences contact first. This results in thermocouple pair TC8-TC38 experiencing the highest value of thermal contact conductance in the initial contact phase. Complete circumferential contact of PT and CT is achieved within 3 seconds of first contact. Model predictions give a peak CHTC value of 6.2 $kW/m^2 \cdot °C$ and an equilibrium value of approximately 1.8 $kW/m^2 \cdot °C$. This shows good agreement with the extracted experimental data which shows peak and equilibrium values of approximately 6.5 $kW/m^2 \cdot °C$ and 1.5 $kW/m^2 \cdot °C$ respectively.

Figure 4.13 is a heat flux plot for the contact transient. The results show a the expected large spike in PT-CT heat flux as well at the CT-moderator heat flux

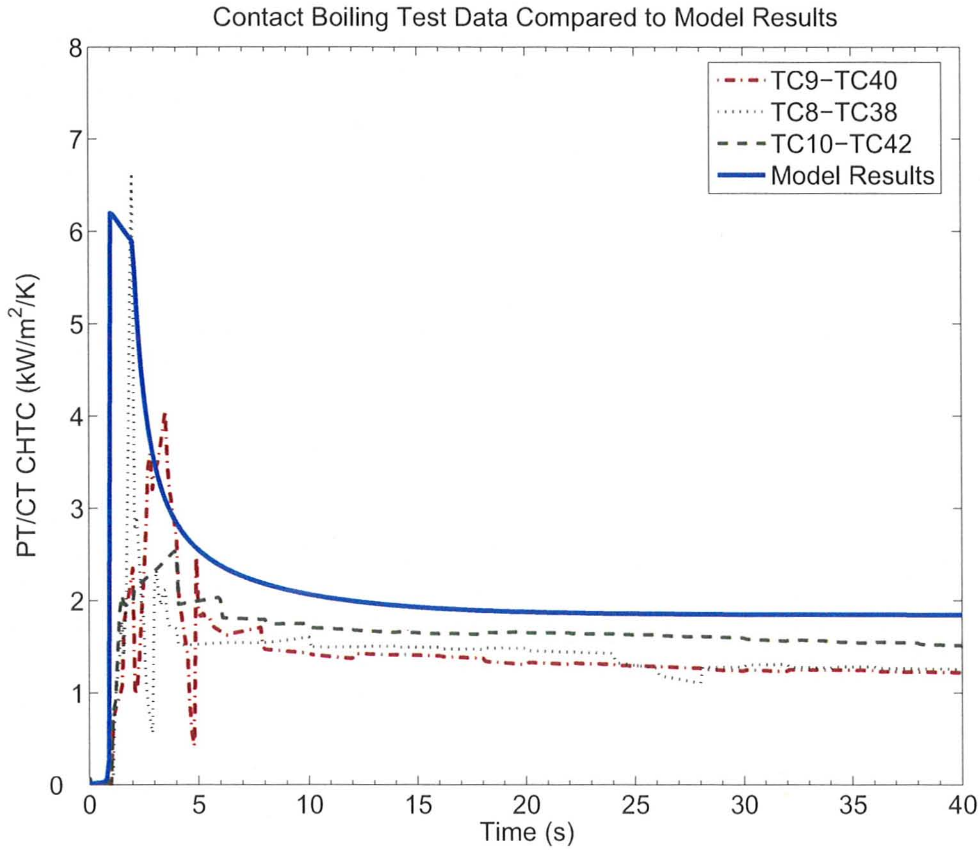

Figure 4.12: Comparison of model predictions to extracted CHTC data from ring 4 of experiment SUBC5

transient. Incident heat flux on the inner PT wall remains relatively constant for the transient duration. This figure illustrates the system reaching equilibrium as all three heat fluxed reach similar values in the post-contact phase. PT-CT heat flux is the amount of heat that is transferred to the calandria tube during the contact event and is the main factor in determining whether fuel channel integrity will be compromised. Although this parameter can spike to a high value at initial contact, it is limited in the post-contact phase. Although it is limited by the PT-CT CHTC, it is also limited by the temperature difference between PT and CT. This temperature difference rapidly decreases after contact is made.

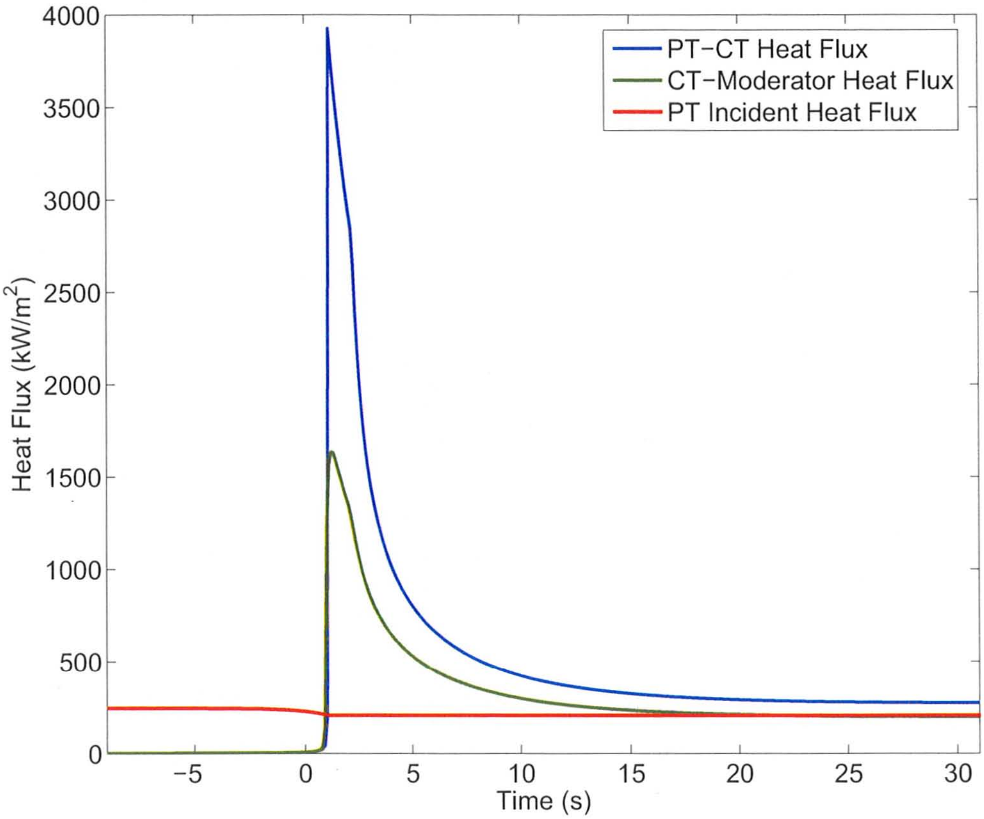

Figure 4.13: Calculated heat fluxes for PT-CT contact transient test SUBC5

4.6.2 Comparison to Data from Fan et al.

The test examined by Fan et al. was classified as experiencing "patchy film boiling" on the CT outer surface. The definition for this classification is that 16-50 % of the CT surface experiences periods of film boiling. This test features a moderate level of subcooling as well as high PT incident heat flux conditions. It was determined that sections of the CT outer surface were in film boiling for approximately 13 seconds before quench. CHTC data from eight thermocouple pairs arranged in two rings on the test section are shown in a plot (H.Z. Fan, 2004). Table 4.4 shown experimental temperatures and predicted temperatures for PT and CT along with calculated boundary condition values used in the code simulation. It can be seen in the table that CT maximum outer surface temperature predictions are in better agreement for the Q6 case. This is because of the CT dryout condition imposed following initial contact in the model.

Table 4.4: Experimental data and model predictions for Q6

	q'_{pt}	h_{conv}	PT Contact Temp	Max CT Temp
Experimental Data			815-862 $°C$	621 $°C$
Model Predictions	78.9 kW/m	16 $kW/m^2 \cdot °C$	784 $°C$	517 $°C$

Figure 4.14 shows the CHTC data along with model predictions for the test (shown by the solid blue line). The time scale is set so that initial contact occurs at time zero. Initial contact is defined as the time when PT temperature reaches a maximum and begins to decrease as it loses heat to the calandria tube. In the model simulation, a dryout condition was imposed from initial contact to 13 seconds after initial contact. This was achieved by adjusting the CT-moderator heat transfer coefficient for the dryout period. The value was decreased to one consistent with film boiling heat transfer. The thermocouple pair most affected by dryout was at location 2-90 as seen in the plot. Model predictions give a peak CHTC value of 7.6 $kW/m^2 \cdot °C$ and an equilibrium value of 2.1 $kW/m^2 \cdot °C$. Experimental values are approximately 7.5 $kW/m^2 \cdot °C$ and 1.2 $kW/m^2 \cdot °C$ respectively. The equilibrium prediction value is approximately twice that of experimental results.

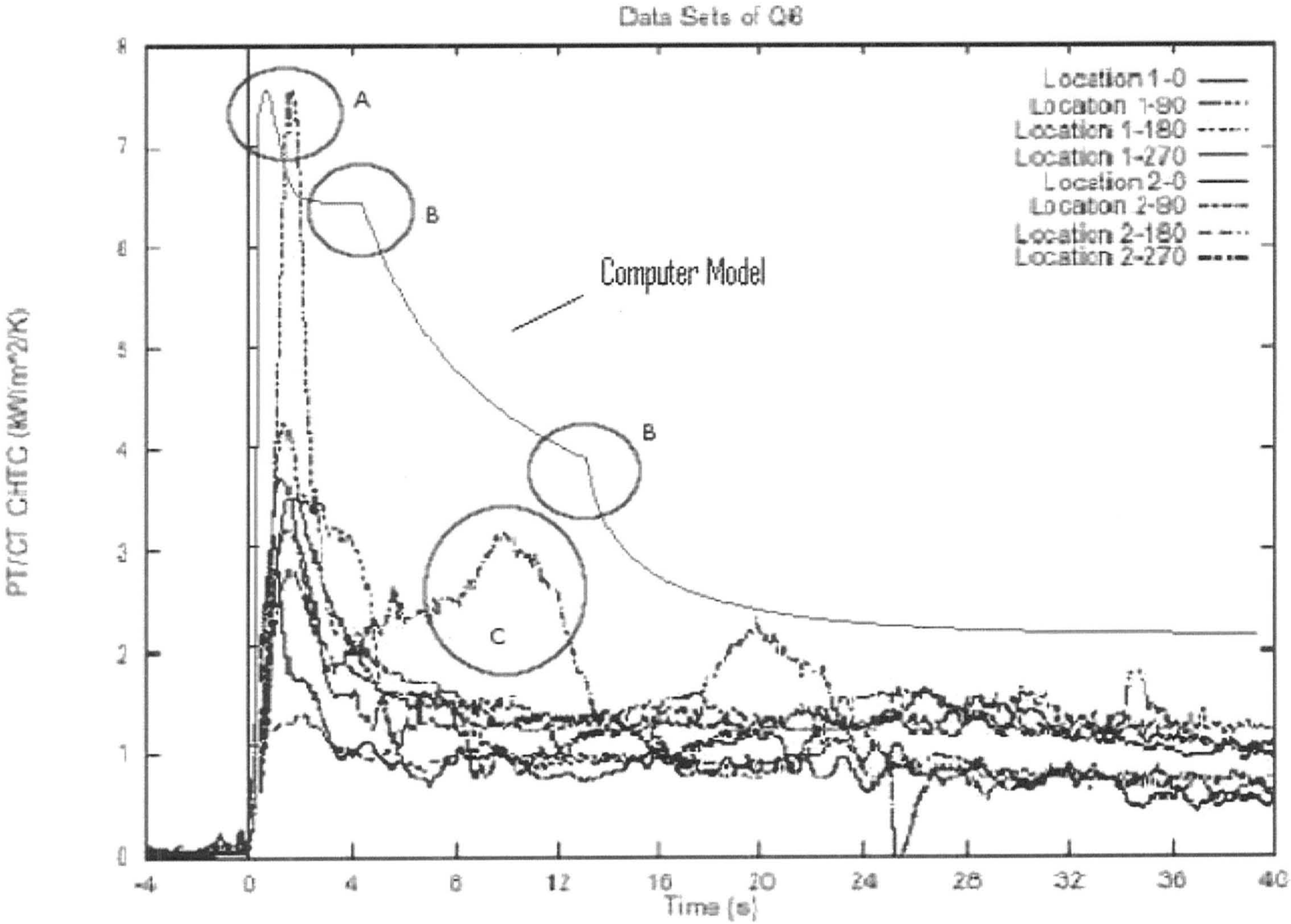

Figure 4.14: Comparison of model predictions (solid blue line) to data extracted by H.Z. Fan (2004) from experiment Q6

There are several regions of interest in figure 4.14 which are labeled in the plot and will be discussed here;

Region A shows the peak TCC values observed in both in the experiment and model. This is the portion of the PT which made first contact with the CT (location 2-90). The model prediction reaches a maximum approximately one second before the experimental results. This can be attributed to both the assumption of rapid interfacial pressure increase as well as the lumped parameter model used in the temperature module. Because in the experimental scenario the interfacial pressure does not reach a maximum instantaneously as in the computer model, peak TCC values are slightly delayed. Also, if the temperature module included a radial conduction term, it would better account for the temperature distribution in the CT. This would result in the bulk CT temperature remaining lower for a slightly longer period of time.

The two regions denoted by the letter B show discontinuities in the model predictions. This is a result of a dryout condition being imposed on the outer CT surface in the model. This is accomplished by reducing the CT-moderator HTC which comes into affect when the CT outer surface exceeds a threshold temperature. In order to agree with the experimental results from Q6, dryout ends after approximately 13 seconds, which accounts for the second discontinuity in model predictions. Before the dryout condition is imposed, the model prediction appears to start to reach an equilibrium value at 6.5 $kW/m^2 \cdot °C$. When dryout occurs, the CT temperature increases significantly and results in high CT creep. This serves to decrease the value of TCC.

Region C shows one thermocouple location (2-180) which appears to have an oscillating TCC value. This location reaches a maximum TCC value at initial contact similar to all other locations but exhibits several other local maxima in the plot. One possible explanation for the oscillations is that this region might be experiencing intermittent dryout. During periods of CT dryout the contact pressure (and likewise HTC) will decrease as the CT temperature increases. After quenching, CT temperature will drop and contact pressure will increase. This type of intermittent dryout is expected to produce results similar to that in region C.

The main reason that peak CHTC values are higher for experiment Q6 is that this test features a higher PT internal pressure. Since harder contact pressure produces a higher value of thermal contact conductance, it is the primary limiting factor for peak CHTC values. It should also be noted that at high PT internal pressures, the PT will balloon into contact more rapidly. This provides less time for PT heatup and results in tests with a higher PT internal pressure having lower PT contact temperatures. Lower PT contact temperatures lead to a lower PT-CT temperature difference at initial contact and a low contact heat flux.

4.6.3 Discussion of Results

For both of the experiments presented in the previous sections the predictions of the mechanistic model are in good agreement and generally reproduce similar values for the CHTC maximum and equilibrium states. It can be seen that the model predictions align with the highest value for TCC when data from multiple thermocouple pairs is shown. This is because in experimental results the portion of the test section that undergoes PT-CT contact first generally experiences the highest value of thermal contact conductance. In the mechanistic model developed here, it is assumed that creep strain is uniform in the radial direction. Therefore contact occurs simultaneously throughout the circumference of the PT-CT interface which produces CHTC values generally higher than at the majority of locations in a real life PT-CT contact event.

It is also observed that PT contact temperature and CT maximum temperature are under predicted by the model. Maximum CT temperature values are taken from thermocouple data for a specific, localized area on the outside of the calandria tube. This means that recorded values are subject to variation from the average CT temperature because of local conditions that may be present such as CT dryout. Since the computer model is a uniform approximation, it was calibrated to align with the point on the test section exhibiting the highest value of contact HTC. This corresponds to the portion of the PT which makes contact with the CT first.

Incident heat flux on the pressure tube plays an important role in the CHTC transient. The P/L ratio (discussed in section 4.3) will decrease for increasing PT incident heat flux. As the system attempts to reach an equilibrium state in the post-contact phase, higher PT incident heat flux causes harder contact pressure between PT and CT. This raises the thermal contact conductance equilibrium value. A sensitivity analysis of incident heat flux was not conducted because it is not one of the key parameters for TCC identified on page 28.

Calandria tube-moderator heat transfer for the two experiments shown was determined by using the Rohsenow correlation (equation 4.6) for pool boiling. The resulting CT-moderator heat transfer coefficient for test Q6 is lower than test SUBC5. This is due to a lower subcooling in Q6 and is most likely the reason this test experienced significantly higher levels of CT dryout.

Table 4.5: Property values used for model predictions

Property	Value
RMS surface roughness (σ)	$11\,\mu m$
RMS surface asperity slope (m)	0.12
PT thermal conductivity (k_{pt})	$18\,W/m{\cdot}K$
CT thermal conductivity (k_{ct})	$13.7\,W/m{\cdot}K$
PT specific heat (C_{ppt})	$350\,J/kg{\cdot}K$
CT specific heat (C_{pct})	$290\,J/kg{\cdot}K$

Chapter 5

Conclusions and Recommendations

A computer model has been developed which simulates the event of a pressure tube heating up and ballooning into contact with the calandria tube in a CANDU reactor. The mechanistic model was developed using proven equations and correlations to describe the three distinct phases in such a postulated event. Results demonstrate transient contact conductance values that are consistent with data taken from contact boiling experiments. During such a transient, high values of PT-CT contact conductance are not sustained for extended periods of time. This is due to factors such as contact pressure, which may be high during the initial contact phase but limits the equilibrium value of TCC in the post-contact phase.

Predicted values from the model bound experimental data in both test. This demonstrates a significant level of conservatism which is often required in safety analysis. Peak CHTC values differ by a maximum of 5% and equilibrium values by a maximum factor of 2. Therefore, the model predicts maximum CHTC values fairly accurately and exhibits a certain degree of conservatism as the system reaches equilibrium.

The sensitivity analysis conducted demonstrates that the effect of surface roughness on solid and gas gap conductivity is at a maximum in the initial contact phase. Roughness sensitivity rapidly decreases for solid contact in the post contact phase but still remains significant for gas gap conductivity. Sensitivity to contact pressure however, has a larger magnitude in the post contact phase especially with respect to gas gap conductivity. This is most likely because gas gap conduction is the dominant mode in the post contact phase. These results illustrate the importance of understanding surface characteristics especially after contact has been made. Sensitivity of TCC to the CT-moderator HTC is seen to have a maximum in the initial contact phase and then decreases significantly in the post contact phase. This most likely occurs due to much lower heat flux incident on the CT in the post contact phase.

This work may be extended by a more detailed study of PT and CT surface characteristics and their specific behaviour during a contact event. Properties such as surface roughness and hardness should be examined for varying temperature and contact pressure. This CANDU specific information would greatly help contact conductance predictions. Specifically, in future contact boiling experiments profilometer traces of PT inner and CT outer surfaces should be performed both before and after testing.

Also, the development of a full one dimensional model would be beneficial for prediction of various effects which arise from the case where PT-CT contact occurs at one location prior to full circumferential contact. The first location to make contact creates a rapid heat redistribution and has a significant effect on subsequent contact occurring at different locations. Such a model could also account for the effects of gravity and how they influence forces on the pressure tube. Incorporating radial temperature equations into the one dimensional model would allow the prediction of temperature distributions in both the pressure and calandria tube which would greatly improve model results.

Bibliography

Ainscough, J. (1982). Gap Conductance in Zircaloy-Clad LWR Fuel Rods,. *OECD, NEA, CSNI Report No. 72.*

Carey, V. (2008). Liquid-Vapor Phase-Change Phenomena,. *Taylor and Francis Group.*

Fong, R. and Chow, C. (2002). High-Temeperature Transient Creep Properties of CANDU Pressure Tubes,. *CNS Annual Conference.*

H.Z. Fan, M. Shams, D. S. (2002). A Methodology to Assess Transient Contact Heat Transfer Coefficient using Contact Boiling Test Data,. *AECL-CONF-1251, CNS Nuclear Simulation Symposium.*

H.Z. Fan, Z. Bilanovic, T. N. (2004). Use of CATHENA to Model Calandria-Tube/Moderator Heat Transfer After Pressure-Tube/Calandria-Tube Ballooning Contact,. *AECL-CONF-01453, CNS Sixth International Conference on Simulation Methods in Nuclear Engineering.*

Incropera, F. and DeWitt, D. (2002). Fundamentals of Heat and Mass Transfer,. *John Wiley and Sons, Inc.*

Lemczyk, T. and Yovanovich, M. (1987). New Models and Methodology for Predicting Thermal Contact Resistance in Compound Cylinders and Finned Tubes,. *Heat Transfer Engineering*, **8**.

Luxat, J. (2002). Mechanistic Modeling of Heat Transfer Processes Governing Pressure Tube-To-Calandria Tube Contact and Fuel Channel Failure,. *CNS Annual Conference*.

Luxat, J. (2008). Dynamic Sensitivity Analysis of Thermal-Mechanical Deformation of a CANDU Fuel Channel,. *16th International Conference on Nuclear Engineering*.

Luxat, J. (2009). Thermal-Hydraulic Aspects of Progression to Severe Accidents in CANDU Reactors,. *Journal of Nuclear Technology*, **167**.

M. Bahrami, M.M. Yovanovich, J. C. (2004a). Thermal Joint Resistances of Conforming Rough Surfaces with Gas-Filled Gaps,. *Journal of Thermophysics and Heat Transfer*, **18**.

M. Bahrami, J.R. Culham, M. Y. (2004b). Modeling Thermal Contact Resistance: A Scale Analysis Approach,. *Journal of Heat Transfer*, **126**.

M.G. Cooper, B.B. Mikic, M. Y. (1969). Thermal Contact Conductance. *International Journal of Heat and Mass Transfer*, **12**.

Mikic, B. (1974). Thermal Contact Conductance; Theoretical Considerations. *International Journal of Heat and Mass Transfer*, **17**.

Mochizuki, H. and Quaiyum, M. (1994). Contact Conductance between Cladding/-Pressure Tube and Pressure Tube/Calandria Tube of Advanced Thermal Reactor (ATR),. *Journal of Nuclear Science and Technology*, **31**.

Neal, P. and Fraser, C. (2003a). Contact Boiling Experiement SUBC3,. *COG-02-2018.*

Neal, P. and Fraser, C. (2003b). Contact Boiling Experiement SUBC5,. *COG-02-2020.*

OPG (2001). Darlington NGS Safety Report, Part 2,.

Patankar, S. (1980). Numerical Heat Transfer and Fluid Flow,. *Hemisphere Publishing Corporation.*

Ross, A. and Stoute, R. (1962). Heat Transfer Coefficient Between Uranium Dioxide and Zircaloy-2. *AECL CFRD-1075.*

R.S.W. Shewfelt, L.W. Lyall, D. G. (1984). A High Temerature Creep Model for Zr-2.5 wt% Nb Pressure Tubes,. *Journal of Nuclear Materials*, **125**.

R.S.W. Shewfelt, L. L. (1988). A High Temerature Creep Model for Zircaloy-2 Calandria Tubes,. *COG-88-37.*

SCDAP/RELAP5 (1997). SCDAP/RELAP5/MOD3.2 CODE MANUAL VOLUME IV: MATPRO - A LIBRARY OF MATERIALS PROPERTIES FOR LIGHT-WATER-REACTOR ACCIDENT ANALYSIS,. *Idaho National Engineering and Environmental Laboratory.*

Shlykov, Y. and Ganin, Y. (1964). Thermal Resistance of Metallic Contacts. *International Journal of Heat and Mass Transfer*, **7**.

Song, S. and Yovanovich, M. (1988). Relative Contact Pressure: Dependence on Surface Roughness and Vickers Microhardness,. *Journal of Thermophysics and Heat Transfer*, **2**.

Yovanovich, M. (1981). New Contact and Gap Conductance Correlations for Conforming Rough Surfaces,. *AIAA Paper No. 81-1164, AIAA 16th Thermophysics Conf., Palo Alto, Calif.*

Yovanovich, M. (2006). Micro and Macro Hardness Measurements, Correlations, and Contact Models,. *44th AIAA Aerospace Sciences Meeting and Exhibit.*

Appendix A

Time Step Analysis

When using an explicit discretization scheme, it is important to use a small enough time step. Time steps which are too large can yield unrealistic results (Patankar, 1980). The following presents an analysis that justifies the time step of 0.1 seconds used in computer simulations. Figure A.1 shows several CHTC transients obtained by simulations with different time step values. It can be seen that at larger time steps the transient curve is shifted due to the inaccuracy in the explicit discretization scheme. There is a large difference in the calculated transient between time steps of 5 seconds and 0.1 seconds. The difference however, is notably small between time steps 0.1 seconds and 0.01 seconds. This leads to the conclusion that a time step smaller than 0.1 seconds is unnecessary and results in a needless increase in computational intensity. Another observation that can be made is that the code results are generally very stable. Even though inaccuracies arise from too large a time step, the CHTC transient retains its general characteristics.

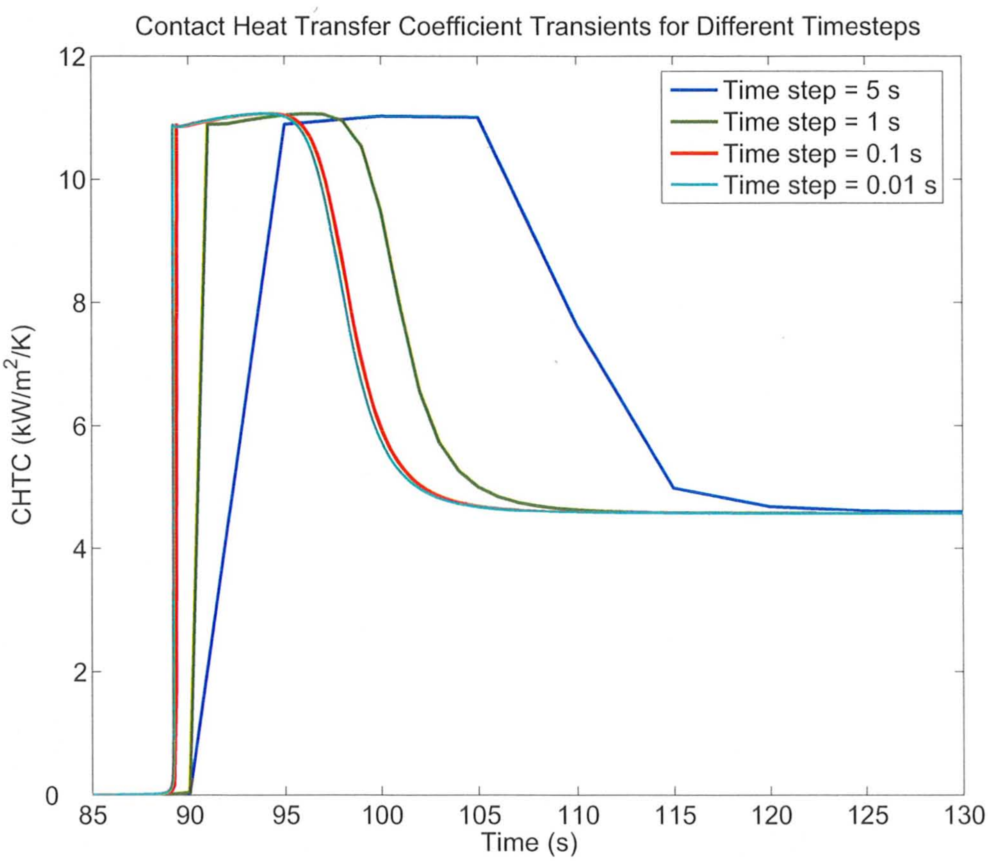

Figure A.1: Comparison of CHTC transients obtained from model using different time steps

Appendix B

TCC Model Development

B.1 Solid Conductance

This section presents more detailed information about the derivation of the Yovanovich thermal contact conductance model. The model is developed by assuming a Gaussian distribution for surface asperity height. The fraction of the surface actually in contact, A_r, over the total apparent contact area of the two surfaces, A_a, can be estimated by the complimentary error function:

$$erfc(x) = 1 - erf(x) = \frac{2}{\sqrt{\pi}} \int_x^{\infty} e^{-t^2} dt \tag{B.1}$$

If $x = \frac{Y}{\sqrt{2}\sigma}$, then the complimentary error function represents the probability that a measurement lies outside $\pm Y$ in a Gaussian distribution with standard deviation σ. This can be applied to determine actual contact area where Y represents mean plane separation of the two surfaces and σ represents surface roughness. From (Yovanovich, 1981);

$$\frac{P}{H} = \frac{A_r}{A_a} = \epsilon^2 = \frac{1}{2} erfc\left(\frac{Y}{\sqrt{2}\sigma}\right) \tag{B.2}$$

The contact pressure to hardness ratio is considered to be a direct representation of the ratio of actual to apparent contact area. Equation B.2 gives a needed relationship between x and P/H. The thermal resistance due to constriction at a single contact spot, i, is;

$$R_{ci} = \frac{\psi_c i}{2k_s a_i} \tag{B.3}$$

Where a_i is the contact spot radius and $\psi_c i$ is the contact spot constriction parameter. For multiple contact spots in parallel;

$$\frac{1}{R_c} = \sum_{i=1}^{N} \frac{1}{R_{ci}} = 2k_s \sum_{i=1}^{N} \frac{a_1}{\psi_c i} \tag{B.4}$$

Converting to contact conductance;

$$h_c = \frac{2k_s}{A_a} \sum_{i=1}^{N} \frac{a_i}{\psi_{ci}} \tag{B.5}$$

Yovanovich (1981) defines a contact conductance parameter derived from a geometric analysis;

$$\sum_{i=1}^{N} \frac{a_i}{A_a} = \frac{1}{4\sqrt{2\pi}} \frac{m}{\sigma} exp(-x^2) \tag{B.6}$$

Equations B.2, B.5 and B.6 can be combined to yield;

$$\frac{\sigma h_c}{k_s} = \frac{m}{2\sqrt{2\pi}} \frac{exp(-x^2)}{(1-\epsilon)^{1.5}} \tag{B.7}$$

Where $x = erfc^{-1}(2P/H)$ and $\epsilon = \sqrt{P/H}$. The final expression for solid contact conductance shown in equation 2.15 is given as a correlational approximation to equation B.7. It should be noted that this result is very close to equation 2.6 developed by M.G. Cooper (1969). This equation was obtained by developing a dimensionless form of contact conductance and comparing it to experimental data as a function of contact pressure to hardness ratio (figure 2.2).

B.2 Gas Gap Conductance

The Yovanovich gas gap term, like most TCC models is based on conduction through the gas. Thermal conductivity of the gas is the most important parameter. The Yovanovich model makes innovations in the correction term as well as the expression for mean plane separation. The correction term is developed as a way to approximate the jump distances normally used for gap conductance (Ainscough, 1982). The expression for mean plane separation (equation 2.17) comes from a correlation which approximates equation B.2.

Appendix C

Contact Boiling Test Dryout Maps

The following are dryout maps of the CT outer surface from each of the two contact boiling tests used in section 4.6. The coloured areas represent areas locations where film boiling occured during the test. Thermocouple locations are marked and the thermocouples used for comparison purposes are indicated.

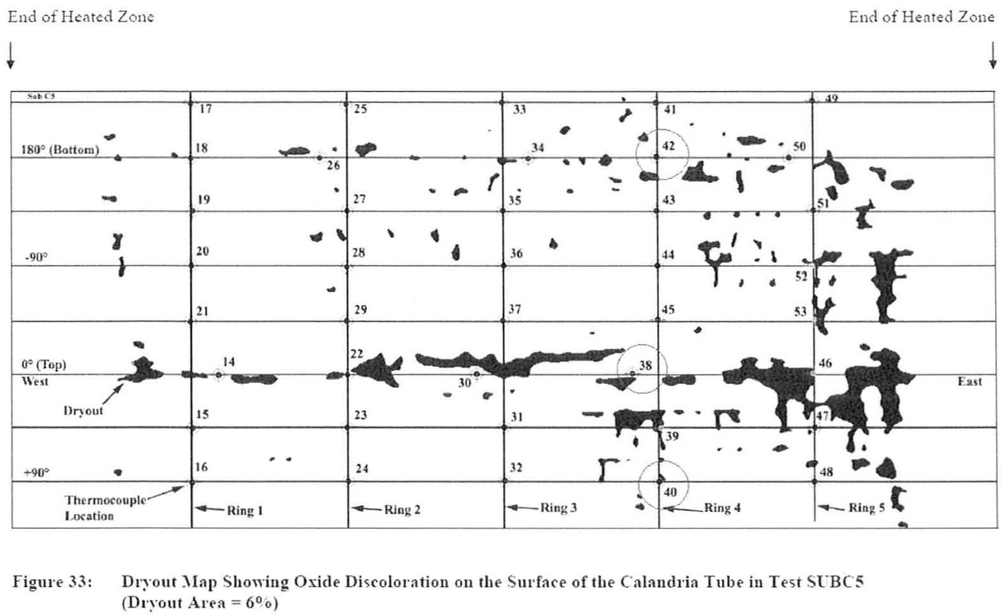

Figure 33: Dryout Map Showing Oxide Discoloration on the Surface of the Calandria Tube in Test SUBC5 (Dryout Area = 6%)

Figure C.2: Dryout map for test SUBC5 (Neal and Fraser, 2003b) with locations of thermocouples circled

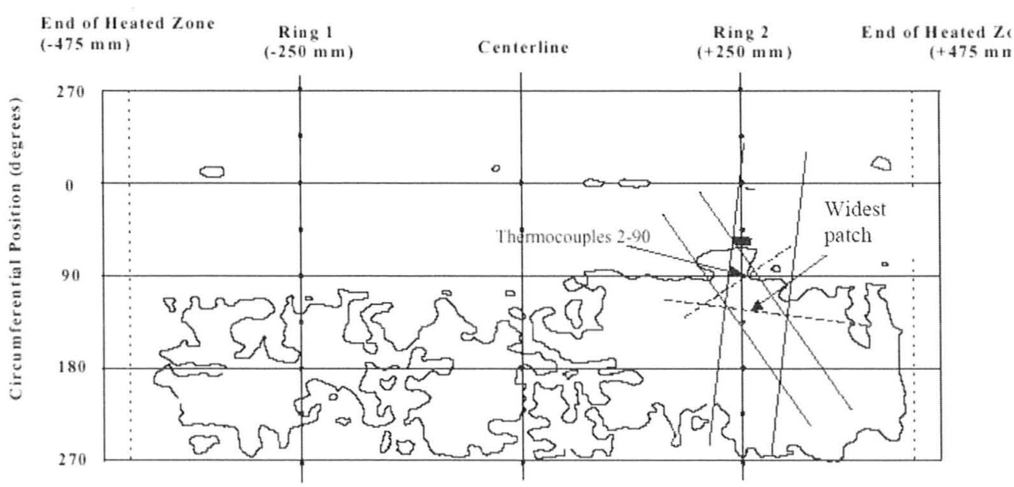

Figure C.3: Dryout map for test Q6 (H.Z. Fan, 2004) with location of thermocouple 2-90 labeled

Appendix D

MATLAB code

The following is the main MATLAB code used to simulate the PT-CT contact transient. The main script is where the code is run from and calls all other scripts.

```
%%%Main Program%%%
clear
%reads input values
input
%main loop
for t=ΔT:ΔT:ttrans
    for i=1:3
        %calculate contact conductance
        Conductance
        if contactflag==0
            marker=step;
        end
        %introduces dryout at initial contact
        %by changine CT-mod HTC
```

```
if contactflag==1
    %hconv=1000;
    hconvl=2*pi*rct*hconv;
    %determines how many timesteps dryout occurs for
    if step-marker≥130
        hconv=26000;
        hconvl=2*pi*rct*hconv;
    end
end
if step>1
    %iteratively solve for PT and CT temperatures
    TempSolve
    %gas conductivity correlation
    kg=(9.460*10^-6)*((PTtemp(step)+CTtemp(step))/2)^1.312;
    %hardness correlation
    Hard=[exp(26.034+PTtemp(step)*(-0.026394+PTtemp(step)...
        *(0.000043504-PTtemp(step)*(0.000000025621))))]/(10^6);
    %tracking variables for gas conductivity and hardness
    kgtrack(step)=kg;
    Hardtrack(step)=Hard;
end
%iteratively solve for contact pressure
Strain
%determines contact microhardness
if contactflag==1
        contacthard2
end
%calculate heat fluxes
%CT-mod heat flux
```

```
        qmod(step)=hconv*(CTtemp(step)-Tl);
        %CT-PT heat flux
        qjoint(step)=HTC(step)*(PTtemp(step)-CTtemp(step));
        %PTincident heat flux
        qptinc(step)=qpt/(2*pi*(rpt-0.5*tpt));
    end
    %change the thickness and radius of tubes as they deform
    rpt=rpto*(1+PTstrain(step));
    tpt=tpto/(1+PTstrain(step));
    rct=rcto*(1+CTstrain(step));
    tct=tcto/(1+CTstrain(step));
    %increment step counter
    step=step+1
end

%plot results
subplot(2,2,1)
plot(time,Pitrans)
subplot(2,2,2)
plot(time,HTC)
subplot(2,2,3)
plot(time,PTtemp,time,CTtemp)
```

The input file contains initial conditions and variable values necessary at the start of the simulation.

```
%%%input file/initial conditions%%%

%time of transient [s]
```

```
ttrans=100;
%timestep size  [s]
ΔT=0.1;
%number of timesteps
n=ttrans/ΔT;
%calculate timescale
for i=1:n+1
    time(i)=i*ΔT−ΔT;
end
%pressure tube internal pressure  [MPa]
Ppt=4;
%calandria tube external pressure  [MPa]
Pext=0.1;
%PT and CT thicknesses  [m]
tpto=0.00424;
tpt=tpto;
tcto=0.0014;
tct=tcto;
%PT and CT radius  [m]
rpto=0.05169+0.5*tpt;
rpt=rpto;
rcto=0.064345;
rct=rcto;
%heat flux to PT  [W/m]
%qpt=25000;
%for heatup rate of 10.5
%qpt=33800;
%for heatup rate of 14
%qpt=46000;
```

```
%for heatup rate of 24.6
qpt=78900;
%for heatup rate of 23.4
%qpt=75200;
%for heatuprate of 25
%qpt=80185;
%for heatuprate of 26
%qpt=83392;
%mass of PT and CT per unit length [kg/m]
mpt=9.164;
mc=2;
%specific heat of PT and CT [J/kg/K]
Cppt=350;
Cpc=290;
%thermal conductivity of PT and CT  [W/m/K]
kp=18;
kc=13.7;
%thermal conductivity of co2 gas [W/m/K]
kg=0.03;
%effective surface roughness of zircaloy PT/CT [m]
rough=11*10^-6;
%mean surface asperity slope
m=0.12;
%meyer hardness of zircaloy [MPa]
Hard=1000;

%heat transfer coefficient between CT and moderator  [W/m^2 K]
hconv=26000;
```

```
%calculate linear heat transfer coefficient between CT and moderator
hconvl=2*pi*rct*hconv;

%temperature of moderator  [K]
Tl=350;

%shewfelt correlation constants
A=5.7*10^7;
B=-29200;
C=140;
D=-19000;
E=22000;
F=-34500;
G=110;
H=-3.5*10^10;

%initial PT and CT temperatures  [K]
Tpo=350;
Tco=350;
%initial HTC
HTC=zeros(1,n+1);


%create PT anc CT temperature array
PTtemp=zeros(1,n+1);
CTtemp=zeros(1,n+1);

%input initial temperatures
PTtemp(1)=Tpo;
```

```
CTtemp(1)=Tco;

%initialize creep integral for CT
I(1:n)=0;

%start at step 1
step=1;

%initialize contact pressure as 0
Pi=0;
Pitrans=zeros(1,n+1);

%initial PT strain is 0
PTcreep=0;

%initial CT strain is 0
CTstrain=zeros(n+1,1);

%initialize contact flag (no contact initially)
contactflag=zeros(1,n+1);

%initialize film boiling flag
FBflag=0;

%molecular mass of CO2 and zirc  [kg/kmol]
Mg=44;
Ms=92;
mu=Mg/Ms;
To=273;  %[K]
```

The conductance script is called from the main file and solves for contact conductance using correlations.

```
%%%Yovanovich Contact Conductance calculation


%approximation for prandtl number
Pr=0.03612/kg;
%fluid parameter
beta=1.1/Pr;
%calculate mean free path
mfp=(0.09*10^-6)*((PTtemp(step)+CTtemp(step))/2)/500;
%calculate thermal accomodation coefficients
alpha1=exp(-0.57*((PTtemp(step)-To)/To))*(1.4*Mg/(6.8+1.4*Mg))...
    +(2.4*mu/(1+mu)^2)*(1-exp(-0.57*((PTtemp(step)-To)/To)));
alpha2=exp(-0.57*((CTtemp(step)-To)/To))*(1.4*Mg/(6.8+1.4*Mg))...
    +(2.4*mu/(1+mu)^2)*(1-exp(-0.57*((CTtemp(step)-To)/To)));
accom=((2-alpha1)/alpha1)+((2-alpha2)/alpha2);
%combine PT and CT thermal conductivities
ks=2*kp*kc/(kp+kc);
%calculate solid contact portion of contact conductance
hc(step)=1.25*[ks*m/rough]*[Pi/Hard]^0.95;
%calculate gap width if contact has not been made yet
if contactflag==0
    gap=rct-(rpt+0.5*tpt);
    Y=abs(gap);
%calculate mean plane separation after first contact using Yovanovich
elseif contactflag==1
    Y=1.184*rough*[-log(3.132*Pi/Hard)]^0.547;
```

```
end
%sets flag for PT/CT contact if contact has been made
if gap≤0
    if contactflag==0;
        epsiloncrit=PTcreep;
    end
    contactflag=1;
end
%save mean plane separation values
Yhist(step)=Y;
%calculate gas gap portion of contact conductance if contact has been made
if contactflag==1
    hg(step)=kg/(Y+beta*mfp*accom);
%calculate gas gap portion of contact conductance
%if contact has not been made
else
    hg(step)=kg/Y;
end
%calculate total gap conductance as sum of solid and gas gap conductances
HTC(step+1)=hc(step)+hg(step);
%calculate effective linear contact conductance
heffl(step)=2*pi*rct*[[tpt/(2*kp)+1/HTC(step+1)+tct/kc]^-1];
```

The temperature solving script solves the lumped parameter heat equations for PT and CT to determine the temperatures in each tube.

```
%%%Solver for Temperature in PT anc CT%%%
%set loop counter to zero
counter=0;
```

```
%TempSolve loop
while 1==1
    %increment counter
    counter=counter+1;
    %equations for temperature
    PTtemp(step)=[ΔT*[qpt+heffl(step)*CTtemp(step)]...
        +mpt*Cppt*PTtemp(step-1)]/[mpt*Cppt+ΔT*heffl(step)];
    CTtemp(step)=[mc*Cpc*CTtemp(step-1)+ΔT*heffl(step)*PTtemp(step)...
        +ΔT*hconvl*Tl]/[mc*Cpc+ΔT*heffl(step)+ΔT*hconvl];
    %save results
    PThist(counter)=PTtemp(step);
    CThist(counter)=CTtemp(step);
    %check for convergence
    if counter>1
        if [PThist(counter)-PThist(counter-1)]<0.001
            if [CThist(counter)-CThist(counter-1)]<0.001
                %clear PThist CThist
                break
            end
        end
    end
end
```

The strain script solves the Shewfelt equations for PT and CT simultaneously in order to determine contact pressure.

```
%%%This script uses Shewfelt correlations to determine PT/CT contact%%%
%%%pressure%%%
%if contact has not yet been established calculate PT creep to determine
```

```
%when contact is made
if contactflag<1
    PTstress(step)=Ppt*rpt/tpt;
    %calcualte PT creep strain rate
    PTcsr(step)=(5.7*10^7)*(PTstress(step)^1.8)*exp(-29200/PTtemp(step));
    %calculte total PT strain
    if step≤1
        PTstrain(step)=ΔT*PTcsr(step);
    elseif step>1
        PTstrain(step)=PTstrain(step-1)+(ΔT*(PTcsr(step-1)...
            +PTcsr(step))/2);
    end
    PTcreep=PTstrain(step);
%if contact has been established calculate contact pressure
elseif contactflag==1
    %initialize contact pressure guess
    Pi=1;
    %initialize istress guess for CT
    istress(step)=1;
    %main contact pressure loop
    while 1==1
        if CTtemp(step)≤Tl
            CTstress(step)=0;
        else
            %calculate CT stress from guessed Pi
            CTstress(step)=abs((Pi-Pext)*rct/tct);
        end
        %internal alpha phase stress in CT loop
        while 1==1
```

```
        %calculate CT dislocation creep
        dcreep(step)=E*((CTstress(step)−istress(step))^5.1)...
            *exp(F/CTtemp(step));
        %calculate integral function
        f(step)=G*dcreep(step)+H*(istress(step)^1.8)...
            *exp(F/CTtemp(step));
        if step≤1
            %set integral to zero for first timestep
            I(step)=0;
        else
            %calculate integral value for remaining timesteps
            I(step)=I(step−1)+(ΔT/2)*(f(step)+f(step−1));
        end
        %calculate new alpha phase stress
        newistress(step)=1.4+I(step);
        isresidual=abs(newistress(step)−istress(step));
        if isresidual<0.001
            break
        end
        %calculate new value for alpha stress
        istress(step)=0.99*istress(step)+0.01*newistress(step);
    end
    % calculate grain boundary creep in CT
    gbcreep(step)=C*(CTstress(step)^1.3)*exp(D/CTtemp(step));
    % calculate PT stress from guessed values of gbcreep etc...
    PTstress(step)=abs([(gbcreep(step)+dcreep(step))...
        /(A*exp(B/PTtemp(step)))]^(1/1.8));
    % calculate new Pi
    Pinew=−(PTstress(step)*tpt/rpt)+Ppt;
```

```
        %calculate residuals
        residual=Pinew-Pi;
        %exit if residual is less than...
        if abs(residual)≤0.00001
            Pitrans(step)=Pi;
            %calculate total creep strain of PT
            PTcsr(step)=(5.7*10^7)*((Ppt-Pi)*rpt/tpt^1.8)...
                *exp(-29200/PTtemp(step));
            PTstrain(step)=PTstrain(step-1)+(ΔT...
                *(PTcsr(step-1)+PTcsr(step))/2);
            CTstrain(step)=CTstrain(step-1)+ΔT...
                *(gbcreep(step)+dcreep(step));
            break
        end
        %calculate new interfacial pressure with extreme relaxation
        Pi=0.999*Pi+0.001*Pinew;
    end
end
```